FFIE
Intern rapport E–297
Reference: Job 370/113
Date: August 1979

A COMBINED PROGRAMMED AND ADAPTIVE ANTENNA NULLSTEERING TECHNIQUE

A feasibility study

by

Magne Eggestad and Svend Heier

Approved
Kjeller 9 August 1979

H K Johansen
Superintendent

FORSVARETS FORSKNINGSINSTITUTT
Norwegian Defence Research Establishment
P O Box 25 – N-2007 Kjeller
Norway

FFIE
Intern rapport E–297
Reference: Job 370/113
Date: August 1979

A COMBINED PROGRAMMED AND ADAPTIVE ANTENNA NULLSTEERING TECHNIQUE
A feasibility study

by

Magne Eggestad and Svend Heier

Approved
Kjeller 9 August 1979

H K Johansen
Superintendent

FORSVARETS FORSKNINGSINSTITUTT
Norwegian Defence Research Establishment
P O Box 25 – N-2007 Kjeller
Norway

CONTENTS

A COMBINED PROGRAMMED AND ADAPTIVE ANTENNA NULLSTEERING TECHNIQUE
A feasibility study

SUMMARY

A programmed and adaptive antenna nullsteering technique is described. The method is first described in broad terms. Then follows a more detailed description of the programmed part, the calibration system, the influence of different types of errors, the adaptive loop and the developed algorithm. In the last chapters are given the results of the simulations. The results of the study indicate that the method is well matched to most static radar and communication systems.

1 INTRODUCTION

The concept of interference cancellation of noise entering the side lobes of a radar or communication antenna was originally introduced by Terris and Airs in the mid 1950's at the General Electric Advanced Electronics Centre. Their method was based on incoherent cancellation at video level. In 1956 Paul W Howel extended the ideas to coherent noise cancellation at IF frequencies and patented his work under the title: *IF Side Lobe Canceller* (1).

The coherent side lobe canceller was later developed by Sidney P Applebaum (2) and L E Brennan (3). Today the method is known as Coherent Side Lobe Suppression (CSLS) and has found application in several modern radar systems.

Parallel to the development of CSLS, fundamental theoretical work was conducted by Bryn (4), Mermoz (5), Shor (6), Widrow (7), Griffiths (8) and others on signal processing and adaptive systems in communications and sonar systems. This led to a more general theory of adaptive nullsteering (ANS) of which CSLS was shown to be a special degenerated case.

During the TOR study at the Norwegian Defence Research Establishment the concept of "hardened" landbased 3D surveillance radar systems was introduced. It was then pointed out that the term "hardness" in general could only be justified if the radars also were protected to the same extent against high power stand-off jammers.

A study of the CSLS system revealed that this system was hampered by serious disadvantages which made it less attractive. The more general adaptive method seemed to be well matched to sonar application but less suitable in radar systems where computer speed and capacity were limiting factors.

The spin-off of these studies was a new concept based on programmed null steering for course weight setting and an inner adaptive loop for fine weight adjustments. The concept was first presented in 1976 in two classified NDRE reports (9, 10) and later in 1977 discussed with technical experts at General Electric, Syracuse, and Hughes Aircraft Co, Fullerton, USA.

The primary purpose of the present feasibility study was to select vital and critical parts in the system for closer investigation in order to acquire a better understanding of fundamental parameters and to disclose possible pitfalls in the concept.

The study starts with a rudimentary description of the CSLS and the general ANS system for the purpose of clarification of the physical conditions which led to the programmed null steering concept (PNS).

In Chapters 3, 4 and 5 is given an overall review of the basic operation of the PNS system. These chapters are intended for those readers who only want to acquire a first-hand knowledge of the principles of operation.

Chapters 6, 7 and 9 contain relatively detailed descriptions of the pure programmed part, the adaptive loop operation, data store requirement and the calibration system. Chapter 10 follows with an evaluation of the main error sources. In Chapter 11 are presented the most significant results of the simulations carried out with model antennas and different error sources.

Finally, a rudimentary evaluation is given of system performance when also desired target signal returns are present in the received signal structure.

2 BASIC CHARACTERISTICS OF COHERENT SIDE LOBE SUPPRESSION (CSLS) AND THE GENERALIZED ADAPTIVE NULL STEERING (ANS) TECHNIQUES

2.1 Coherent side lobe suppression

An excellent review of adaptive arrays based on the coherent side lobe suppression technique is given by W F Gabriel in (11). A functional block diagram of multiloop CSLS systems is given in Figure 2.1.

The CSLS system makes use of auxiliary antennas in addition to the main antenna. One auxiliary is needed for each jammer to be cancelled. Provided the received signals through the main antenna side lobes and the auxiliaries at the cross-correlator are coherent, the closed correlation loop will develop a signal structure at the output of the combiner such that all jamming signals received through the main antenna side lobes will cancel in the summing network. This is in fact equivalent to developing nulls or zero points in the main antenna side lobe region in the directions of the jammers. The nulls are directed towards the jammers regardless of main antenna rotation, except when the main lobe is pointing at the jammer. In the last case the CSLS ceases to function.

The main characteristics of CSLS can be summarized as follows:

- It is fully automatic and requires neither manual control nor external reference signals.
- It appears effective against narrow band and stationary noise processes.
- It is not well apt for implementation at RF frequencies.
- Its effectiveness is sensitive to signal decorrelation arising from auxiliary antenna configuration, mismatch in antenna feeders, multipath and clutter.
- Suppression is seriously degraded in wide band radar systems
- It does not cancel or suppress deception jamming.
- If the number of jammers exceeds the number of correlation loops, serious degradation may occur.

– Multiloop systems appear feasible in theory. However, successful realization under realistic jamming conditions has not yet to the author's knowledge been fully demonstrated.

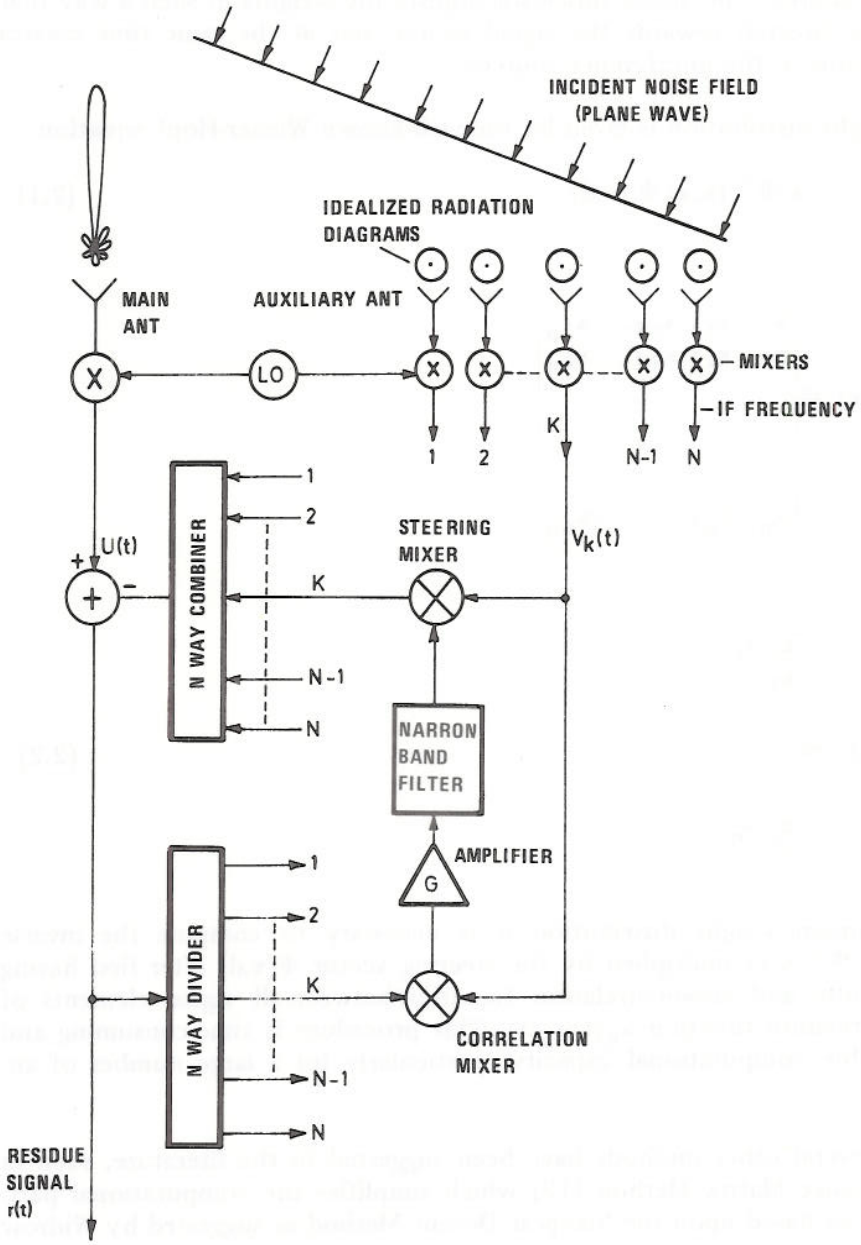

Figure 2.1 Basic multiloop coherent side lobe suppression system

2.2 Adaptive null steering

CSLS is a special case of the more general adaptive null steering (ANS) or beam-forming case (ABF) shown schematically in Figure 2.2. In this case it is required to know *a priori* either the characteristics of the desired signal s(t) or the direction to the desired signal source. The signal processor adjusts the weights in such a way that the main beam is directed towards the signal source and at the same time creates nulls in the directions to the interference sources.

The optimum weight distribution is given by the well-known Wiener-Hopf equation

$$W_{opt} = k\,\Phi^{-1}(x,x)\,\Phi(x,d) \tag{2.1}$$

where

$$\Phi(x,x) \equiv \begin{bmatrix} x_{11} & x_{12} & x_{13} & \cdots & x_{1n} \\ x_{21} & x_{22} & x_{23} & \cdots & x_{2n} \\ & & \vdots & & \\ x_{n1} & x_{n2} & \cdots & & x_{nn} \end{bmatrix}$$

and

$$\Phi(x,d) \equiv \begin{bmatrix} x_1 & s_1 \\ x_2 & s_2 \\ \vdots & \\ x_n & s_n \end{bmatrix} \tag{2.2}$$

To find the optimum weight distribution it is necessary to compute the inverse covariance matrix $\Phi^{-1}(x,x)$ multiplied by the steering vector $\Phi(x,d)$ after first having determined the auto- and cross-correlation functions between all signal elements of x(t) and cross-correlation function $x_k(t)\,s_k(t)$. This procedure is time-consuming and requires considerable computational capacity, particularly for a large number of antenna elements.

For that reason several other methods have been suggested in the literature, such as the Sample Covariance Matrix Method (12) which simplifies the computational part, or iteration methods based upon the Steepest Decent Method as suggested by Widrow *et al* (7).

These methods are all hampered by adaption time constants in the order of milliseconds. Time constants of this order of magnitude may not be critical in low information speed systems such as sonar and some types of data and communication systems, but can generally not be accepted in radar systems where target speeds and information rates are high. Neither the CSLS solution nor the more general adaptive methods are therefore well matched to radar applications.

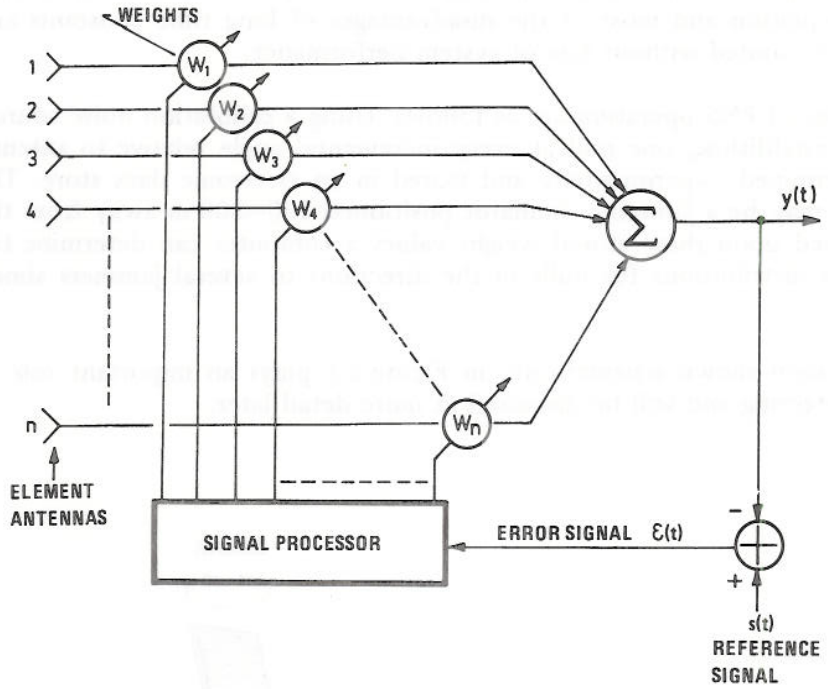

Figure 2.2 Principles of adaptive null steering using multielement arrays

3 PROGRAMMED NULL STEERING (PNS) – BASIC OPERATION

Examination of equations (2.1) and (2.2) reveals the following physical significance of these equations:

– The covariance matrix correlates the different signal sources in space and determines the direction to the interference sources relative to the main antenna boresight axis.

– The steering vector correlates the interference sources with the desired signal such that the main beam can be pointed at the signal source.

In many search radar applications and in particular where the radars are positioned in a reflection-free environment, the directions to the interference sources can be determined quite accurately by conventional methods. Also in the case of Stand Off Jammers (SOJ) the rate of angular change to this interference source is low. Automatic and/or manual strobing facilities are today standard features in most modern radar systems. Evidently, there would be no need to solve the covariance matrix if the directions to the interference sources could be determined by other means and the weight distribution for establishing nulls in those directions were known *a priori.*

Regarding the steering vector, equation (2.2), the main beam is fixed and normally slaved to a mechanical rotation in azimuth. In the case of a 3D radar, the search in elevation is performed electronically in a predetermined pattern. Therefore, main beam steering is fixed and equation (2.2) is not applicable in search radar systems.

In programmed null steering these facts are fully utilized. It is assumed that the jammers appear as point sources in space and that the directions to these interference sources can be determined sufficiently accurately. This eliminates the need for solving the Wiener-Hopf equation and most of the disadvantages of long time constants and large computers are avoided without loss of system performance.

The basic principles of PNS operation are as follows: Using a calibration noise source, weight values for establishing one null at every incremental angle relative to antenna boresight are determined experimentally and stored in an electronic data store. The calibration source may be a jamming simulator positioned 100–300 m away from the radar antenna. Based upon these stored weight values a computer can determine the appropriate weight distributions for nulls in the directions to several jammers simultaneously.

The calibration system shown schematically in Figure 3.1 plays an important role in programmed null steering and will be discussed in more detail later.

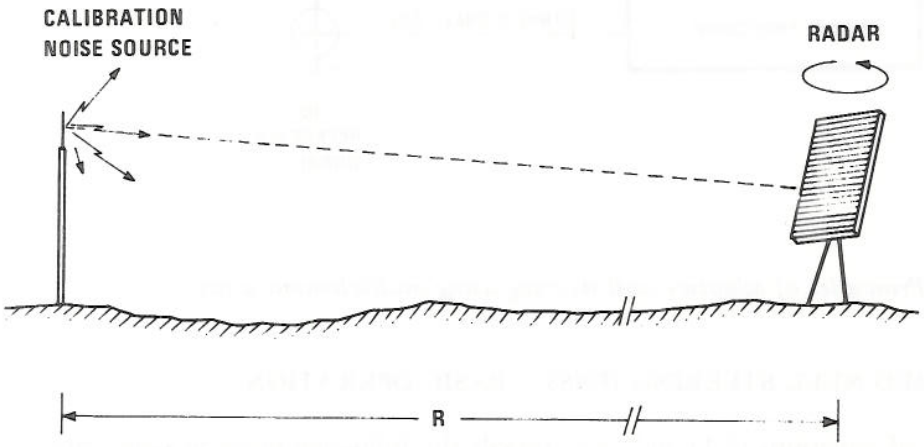

Figure 3.1 Principles of PNS calibration

3.1 The pure programmed part of PNS

Although a 3D radar system is assumed throughout the rest of this paper, PNS can equally well be applied to 2D radar systems. It should, however, be realized that target height information is required regardless of antenna type.

The functional block diagram of PNS is shown in Figure 3.2.

The main antenna output is fed into the T/R switch which normally would be close to the transmitter. In this case the T/R switch is placed in the auxiliary antenna housing.

Like the CSLS, auxiliary antennas are also used in the PNS system. The number of antennas required must be equal to or greater than the number of jammers to be suppressed simultaneously.

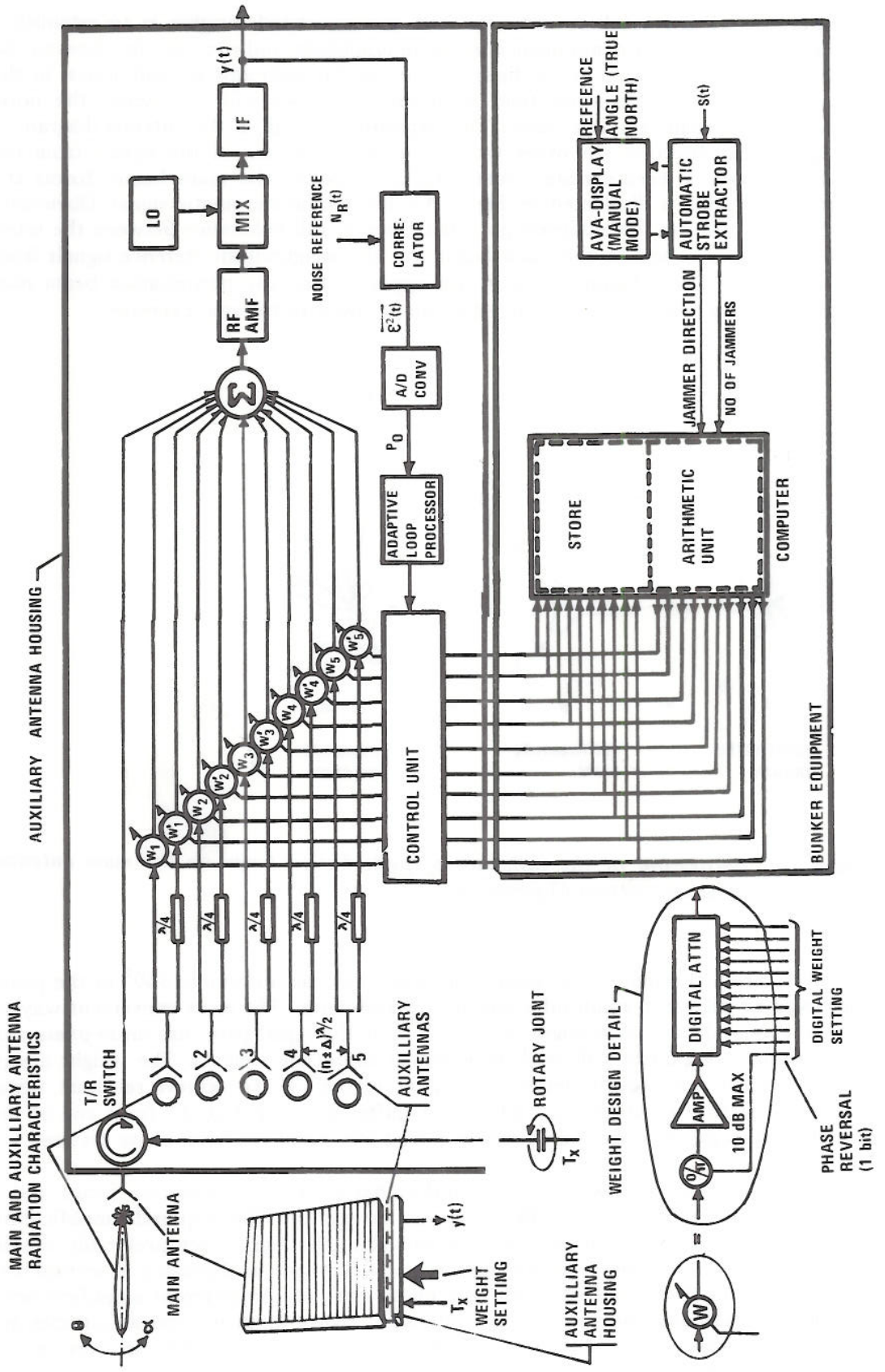

Figure 3.2 Block diagram of the combined programmed and adaptive null steering

The purpose of the auxiliary antennas and the associated weights is to establish a vector field where each component is equal in amplitude and opposite in phase to the corresponding components of the field received in the main antenna side lobes. In the summation network the noise field from the auxiliaries will just cancel the noise received in the main antenna beam. This establishes a null in the antenna diagram in that particular direction. In other words, the weighted sum of the signals from the auxiliaries form a *perturbation beam* which, added to the main beam, forms the desired nulls. This is illustrated in Figure 3.3 for a monochromatic signal. Obviously, cancellation can only be achieved provided there is full coherence between the interference signals received in the main beam and the weighted interference signals from the auxiliaries. From Figure 3.3 it is also apparent that the perturbation beam may distort the main beam if the weight values are allowed to become excessive.

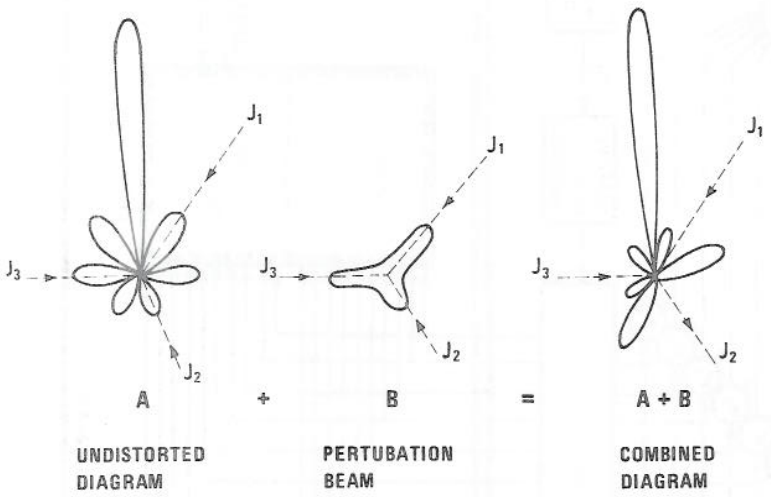

Figure 3.3 Illustration of the influence of perturbation beam on the main antenna radiation pattern (3 jammers)

Signals received through the auxiliary antennas must be adjustable 360° in the phase plane and to different amplitudes within a preset limit. The most convenient way to achieve this at 10 cm wavelength may be to split the signal path into an *in-phase* and a *quadrature* component followed by identical amplitude weights. The weight design is illustrated in the weight detail drawing in Figure 3.2. To achieve resultant signal vectors in all four quadrants, a 180° phase shifter is required at the front end of the amplifier. A negative weight value indicates that the signal has been phase reversed.

The amplifier which follows the phase shifter has a fixed amplification factor and a bandwidth of approximately 10% of centre frequency. The required amplification factor depends primarily on the main antenna side lobe level which preferably should be below –40 dB referred to main antenna maximum gain as discussed in section 6.1. Neither the amplification factors nor the phase shift of the different amplifiers need be equal or within close tolerances. Systematic errors in phase and amplitudes are automatically taken care of by the calibration system as long as they are invariant to attenuator settings.

PIN diode digital attenuators of more than 80 dB range and 0.1 dB resolution are commercially available. Large phase shifts as function of attenuator setting may either be compensated for through phase shift networks or taken care of directly by the computer.

The direction to the jammers is fed into the computer by an automatic strobe extractor. Direction information may also be given manually by using an AVA-display. As convenient reference direction in azimuth (α) true North may be chosen.

Direction to a strong jammer can be determined to an accuracy better than 1/10 of the main antenna beamwidth referred to the half-power points.

3.2 The adaptive part of PNS

Following the hybrid summing circuit is an RF amplifier stage, the local oscillator and an IF amplifier which is band-limited and matched to the transmitted radar signal. The output signal y(t) will in case of jamming contain the desired signal s(t), a thermal noise level $N_t(t)$ and the interference signal $N_j(t)$. That is

$$y(t) = s(t) + N_j(t) + N_t(t) \tag{3.1}$$

Considering side lobe jamming only, the signal component in equation (3.1) can be disregarded for the time being. The output noise signal y(t) is in a noise power detector compared to a reference noise level $N_r(t)$. The output error signal $\epsilon^2(t)$, being proportional to the average jamming signal power, is fed via an analogue-digital converter to a signal processor. Dependent upon the output power level P_0 the processor gives a command to change the weight setting of one of the weights a certain amount and the resulting change ΔP in the output power P_0 is stored. This is repeated for each weight in time sequence. On the basis of these measurements the gradient

$$\nabla P_0/W = (\Delta P_1/W_1, \Delta P_2/W_2, ...\Delta P_n/W_n) \tag{3.2}$$

is determined and the computer calculates the weight distribution of the first iteration.

This procedure is repeated continuously until the noise output level has been reduced to thermal noise level or until the programmed part sets a new weight distribution.

This algorithm is known as the *Steepest Descent Method* and defines the fewest number of iterations necessary to reach a certain noise level.

The important function of the adaptive part is twofold:

a) There will always be small errors in the position of a programmed null relative to the direction to the jammer. These errors arise from inaccurate direction determination, phase variations *vs* attenuator setting, phase and direction errors due to multipath, numeric computer errors, etc. The closed loop tends at any instant of time to move the minimum point in the direction of the jammer.

b) Under calibration the closed loop is used to determine experimentally the weight values for suppression of the simulator noise source at each incremental solid angle in the complete azimuth plane and up to a certain elevation angle θ.

For further details on the adaptive loop design and operation, the reader is referred to Chapter 7.

4 THE CALIBRATION SYSTEM

For calibration one simulator noise source is used. Assuming that the noise source is properly positioned, the nullsteering system would know no difference between this simulator and a real distant stand-off jammer.

Since only one auxiliary antenna is needed to suppress a single jammer, the two weights associated with each auxiliary are adjusted until the simulator noise power is suppressed below a predetermined level according to the following procedure.

Starting with auxiliary antenna No 1 the control unit allows the adaptive loop to operate on all bits of W_1 and W_1'. All other weights are inhibited or disabled during this operation. Based upon the steepest descent algorithm the closed loop will find the weights W_1 and W_1' which will suppress the simulator noise source to approximately the radar thermal noise level $N_t(t)$. The resulting weight values W_1 and W_1' are then stored in the computer.

Next, auxiliary antenna No 2 is selected and the associated weights W_2 and W_2' are adjusted for simulator noise cancellation in exactly the same manner and the resulting weight values W_2 and W_2' stored.

This procedure continues until all individual weight pairs from 1 to N are being determined and stored.

Calibration of the k'th auxiliary antenna for one particular relative direction is illustrated in Figure 4.1. Assuming a CW calibration signal, the received vector in the main antenna side lobe is designated $\bar{R}$. In the coordinate system of Figure 4.1b $\bar{R}$ has been arbitrarily chosen along the real y-axis. Let $\bar{r}_k$ and $\bar{r}_k'$ be the signal vectors received through the k'th auxiliary antenna where the superscript denotes the signal vector in the $\lambda/2$ delayed branch. The relative amplitudes and phases with respect to $\bar{R}$ are arbitrarily chosen.

It is then evident from the vector diagram of Figure 4.1 that the appropriate weight values W_k and W_k' are found by extending the r_k and r_k' vectors until intersecting the circle with radius $|\bar{R}|/2$ in the lower half plane. Then the vector sum

$$W_k\bar{r}_k + W'_k\bar{r}'_k = -\bar{R} \tag{4.1}$$

gives full cancellation of the noise vector $\bar{R}$.

It is also noted that the sine and cosine to the phase angle ϕ_k is given by

$$\sin\phi_k = -\frac{W'_k}{\sqrt{W_k^2 + W'^2_k}} \tag{4.2}$$

$$\cos\phi_k = -\frac{W_k}{\sqrt{W_k^2 + W'^2_k}} \tag{4.3}$$

The relative amplitudes of $\bar{R}$ and $\bar{r}_k$ are given by

$$\frac{|\bar{R}|}{|\bar{r}_k|} = \sqrt{W_k^2 + W_k'^2} \tag{4.4}$$

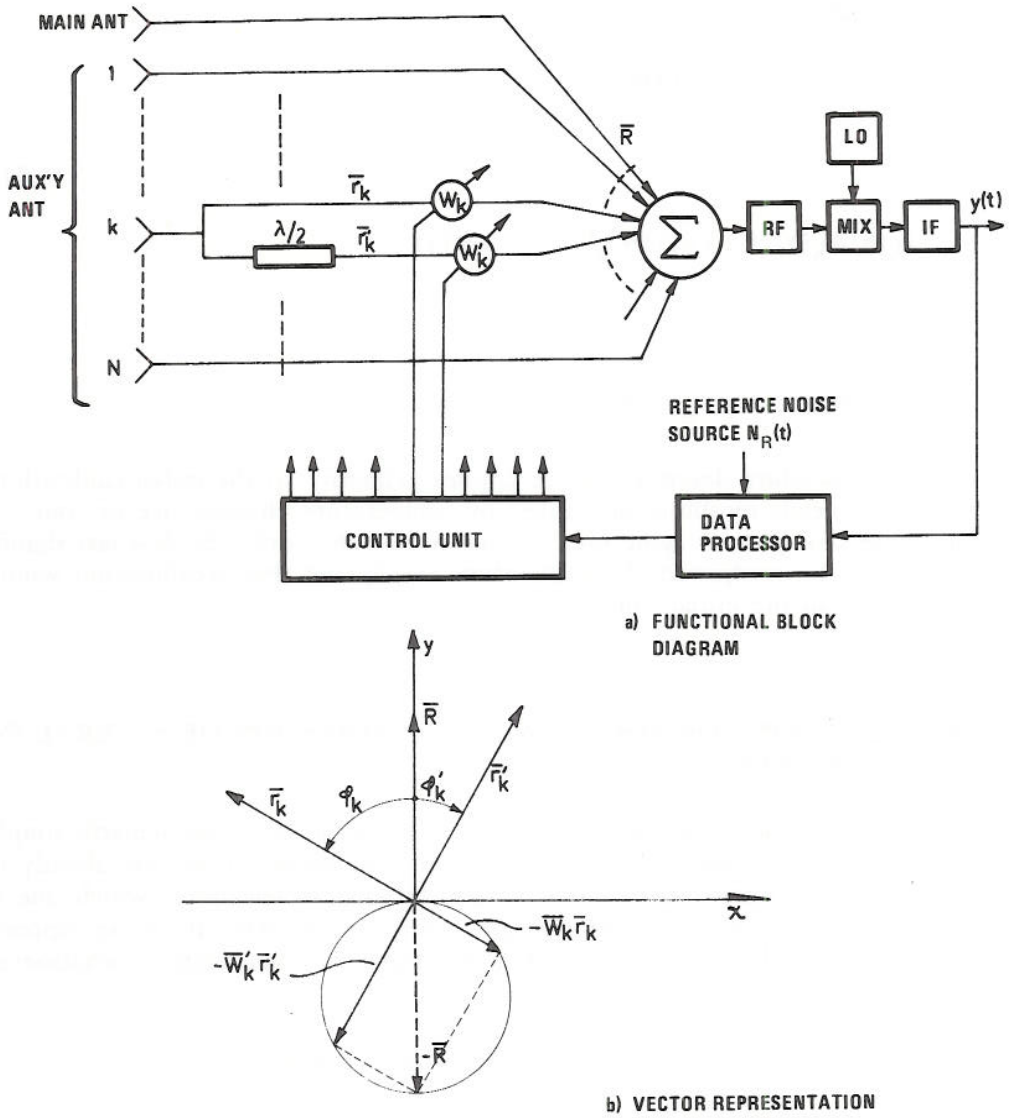

Figure 4.1 Functional block diagram and vector representation of the k'th auxiliary antenna calibration

As the main antenna moves an incremental angle $\Delta\alpha$ in azimuth or an incremental angle $\Delta\theta$ in elevation, a new set of weight values for noise cancellation is determined and stored. This procedure continues until complete sets of weight values giving full noise cancellation for all solid angle increments $\Delta\gamma$ in question are determined and stored.

This completes the calibration.

If γ denotes an arbitrary look angle within the solid angle increment $\Delta\gamma$, the calibrated weights W can be expressed in the following sets of equations

$$\begin{aligned}
&\overline{r_1(\gamma)}W_1(\gamma) + j\,\overline{r'_1(\gamma)}W'_1(\gamma) = -\bar{R}(\gamma)\\
&\overline{r_2(\gamma)}W_2(\gamma) + j\,\overline{r'_2(\gamma)}W'_2(\gamma) = -\bar{R}(\gamma)\\
&\qquad\vdots\\
&\overline{r_k(\gamma)}W_k(\gamma) + j\,\overline{r'_k(\gamma)}W'_k(\gamma) = -\bar{R}(\gamma)\\
&\qquad\vdots\\
&\overline{r_n(\gamma)}W_n(\gamma) + j\,\overline{r'_n(\gamma)}W'_n(\gamma) = -\bar{R}(\gamma)
\end{aligned} \qquad (4.5)$$

The calibration procedure described above applies primarily to the *initial* calibration. When the system needs recalibration caused by temperature changes, ice or rain on antenna aperture, component aging etc, it is presumed that only the few last significant bits have to be readjusted. It is therefore anticipated that recalibration would require less time than the initial calibration.

5 THE BASIC EQUATION FOR SIMULTANEOUS SUPPRESSION OF SEVERAL INTERFERENCE SOURCES

In case only one jammer appears on the scene, the situation is particularly simple since calibrated weight values for suppression of one interference source are already in the store. In this degenerate case one auxiliary antenna is selected – which one is rather immaterial – and the appropriate weight values are extracted for noise suppression in any direction relative to main antenna boresight. No computations whatsoever are involved.

When two or more jammers appear the situation is more complex.

Syppose two interference sources are present. The two interference signals are received by both auxiliary antennas and the resultant weighted vectors from both auxiliary channels must cancel the interference signal $\bar{R}_1$ and R_2 received in the main channel. The vector diagrams in Figure 5.1 a and b illustrate the situation.

Again we have arbitrarily chosen the reference frame such that the main channel interference vector R is directed along the y-axis.

For cancellation of $\bar{R}_1$ and $\bar{R}_2$ the following equations must be satisfied

$$\begin{aligned}
&W_1|r_{1\,1}|\cos\phi_{1\,1} + W'_1|r'_{1\,1}|\cos(\phi_{1\,1}-\overline{\pi}/2)\\
&+ W_2|r_{1\,2}|\cos\phi_{1\,2} + W'_2|r'_{1\,2}|\cos(\phi_{1\,2}-\overline{\pi}/2) - R_1 = 0
\end{aligned} \qquad (5.1)$$

$$\begin{aligned}
&W_1|r_{1\,1}|\sin\phi_{1\,1} + W'_1|r'_{1\,1}|\sin(\phi_{1\,1}-\overline{\pi}/2)\\
&+ W_2|r_{1\,2}|\sin\phi_{1\,2} + W'_2|r'_{1\,2}|\sin(\phi_{1\,2}-\overline{\pi}/2) = 0
\end{aligned} \qquad (5.2)$$

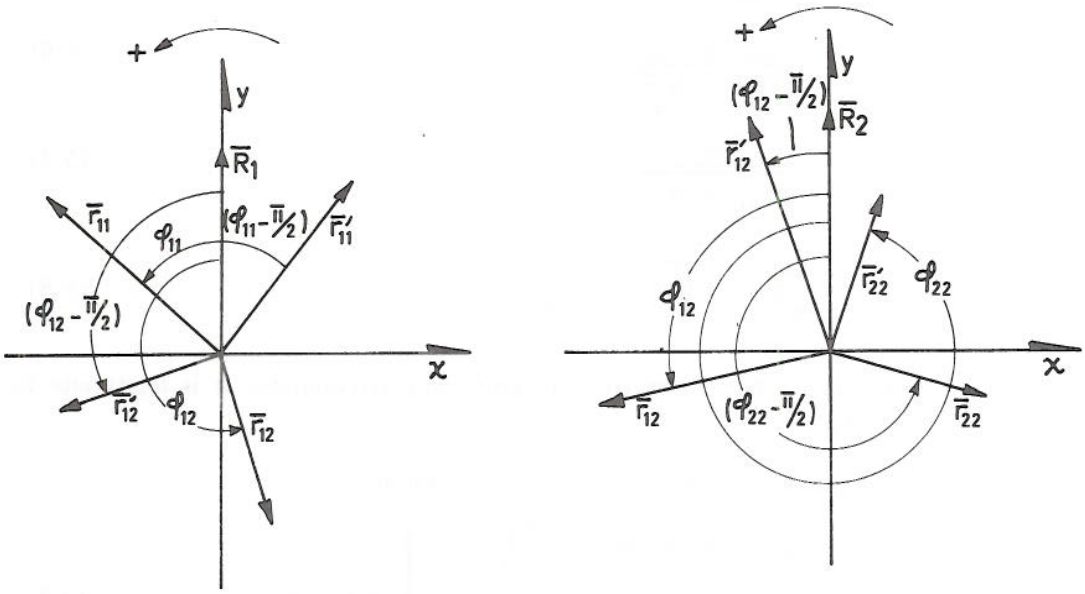

a) SUPPRESSION OF INTERFERENCE SOURCE 1

b) SUPPRESSION OF INTERFERENCE SOURCE 2

Figure 5.1 Vector constellation for suppression of two interference sources

$$W_1|r_{21}|\cos\phi_{21} + W'_1|r'_{21}|\cos(\phi_{21}-\pi/2) + W_2|r_{22}|\cos\phi_{22} + W'_2|r'_{22}|\cos(\phi_{22}-\pi/2)-R_2 = 0 \quad (5.3)$$

$$W_1|r_{21}|\sin\phi_{21} + W'_1|r'_{21}|\sin(\phi_{21}-\pi/2) + W_2|r_{22}|\sin\phi_{21} + W'_2|r'_{22}|\sin(\phi_{22}-\pi/2) = 0 \quad (5.4)$$

The two first equations relate to interference source 1 and the two latter to source 2.

The double indices of r and ϕ refer to the number of auxiliary antenna and to the number of interference sources respectively counted from a reference direction and in a defined direction of rotation.

Generally, for n interference sources and n auxiliary antennas, the equations can be expressed in the following form

$$\left.\begin{aligned}\sum_{i=1}^{n}(W_i|r_{ij}|\cos\phi_{ij} + W'_i|r'_{ij}|\sin\phi_{ij})-R_j &= 0\\ \sum_{i=1}^{n}(W_i|r_{ij}|\sin\phi_{ij} - W'_i|r'_{ij}|\cos_{ij}) &= 0\end{aligned}\right\}\text{for } j=1,2...n \quad (5.5)$$

From equations (4.2), (4.3) and (4.4) the sine and cosine functions and also the relative amplitudes of $|R|$ and $|r|$, determined by the calibrated weight values W_{ij} and W_{ij}' can be expressed in a generalized form

$$\sin \phi_{ij} = -\frac{W_{ij}'}{\sqrt{W_{ij}^2 + W_{ij}'^2}} \tag{5.6}$$

$$\cos \phi_{ij} = -\frac{W_{ij}}{\sqrt{W_{ij}^2 + W_{ij}'^2}} \tag{5.7}$$

$$\frac{|R_j|}{|r_{ij}|} = \frac{|R_j|}{|r_{ij}'|} = \sqrt{W_{ij}^2 + W_{ij}'^2} \tag{5.8}$$

Since a $\lambda/4$ delay line is too short to give significant attenuation, it is legitimate to assume that $|r_{ij}| \equiv |r_{ij}'|$.

The final form of equations (5.5) may then be written as

$$\left.\begin{aligned} \sum_{i=1}^{n} (W_i \cos \phi_{ij} + W_i' \sin \phi_{ij}) - \frac{|R_j|}{|r_{ij}|} &= 0 \\ \sum_{i=1}^{n} (W_i \sin \phi_{ij} - W_i' \cos \phi_{ij}) &= 0 \end{aligned}\right\} \text{for } j=1,2...n \tag{5.9}$$

By substituting (5.6), (5.7) and (5.8) into equation (5.9) it appears that the correct weight distribution for simultaneous cancellation of all interference sources can be found by solving the 2xn linear equations given by (5.9). If 5 interference sources are present at the same time 10 equations have to be solved for each increment angle $\Delta\gamma$ of the main antenna movement.

Two interesting features of PNS operated in this way are immediately noted. It is not required to determine the vectors r and R separately. The only requirement is to establish their ratios which are given by the calibrated weight values. Likewise variations in the amplifier gain, phase shifts and auxiliary antenna radiation diagrams are automatically taken care of through calibration.

6 DETAILED DESCRIPTION OF PROGRAMMED PART – FUNCTIONS AND REQUIREMENTS

In the following sections we will discuss in more detail characteristics and requirements of those parts of the system which are related to the pure programmed part of PNS. Chapter 7 will be devoted entirely to the adaptive inner loop.

6.1 Main antenna average side lobe level requirements

Although PNS is primarily intended for use with 3D radars, it can in principle equally well be applied to 2D radar systems. In both cases elevation as well as azimuth angles to the jammer must be accurately measured. In 2D radar systems height information must be supplied by the height finder radar.

The average side lobe level of the main antenna should be low for the following reasons:

a) Received reflected energy from an interference source via surrounding terrain should preferably in worst case not exceed the radar thermal noise level.

b) Low side lobes will reduce calibration errors due to ground reflection.

c) It is important that the radiation pattern is invariant to antenna rotation. Low side lobe levels in the vertical plane would reduce the antenna coupling to the environment.

d) Low side lobe levels in both planes will reduce weight amplifier requirements and consequently the auxiliary antennas distortion beam.

Ground reflections into the radar antenna side lobes are illustrated in Figure 6.1.

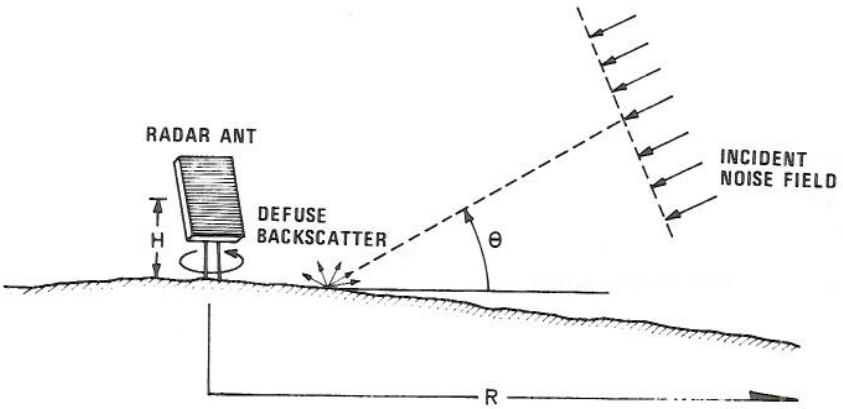

Figure 6.1 Diffuse backscatter from ground of an incident electromagnetic field

At low incident field angles θ total reflections from the ground may be assumed. Also, it is reasonable to assume that rough mountaneous terrain gives rise to diffuse scattering at 10 cm wavelength.

Based on this simplified model, the requirements stated under point a above, the required average side lobe level g is given by

$$\bar{g} \leqslant \frac{16\pi^2 \, R_j^2 \, kT \, F_n}{G \, \lambda^2 \, \sigma \sin\theta} = \ln(R/H) \qquad (6.1)$$

where
- R_j = distance to interference source (m)
- k = Bolzmann's constant = $1.37 \cdot 10^{-23}$ J/K
- T = temperature = 300 K
- F_n = radar noise figure referred to receiver input
- G = radar antenna maximum gain
- λ = wavelength (m)
- θ = incident wave angle (deg)
- σ = noise source effective radiated power density (W/Hz)

By inserting R_j = (classified), R = 10 km, H = 5 m, T = 300 K, F_n = 6 dB, G = 37 dB, $\theta = 5°$, σ = (classified), we find

$$\bar{g} \leqslant -39.1 \text{ dB}$$

indicating that the average side lobe level should be in the order of –40 dB.

Based upon this figure for $\bar{g}$ we may now proceed a step further and calculate the required notch depth g_n such that the noise power received directly through this notch is equal to the scattered noise power from the surrounding terrain. Under worst case conditions this, in fact, means that the receiver noise power has been increased to three times the thermal noise power, resulting in a detection range reduction of 30%. Figure 6.2 illustrates the situation.

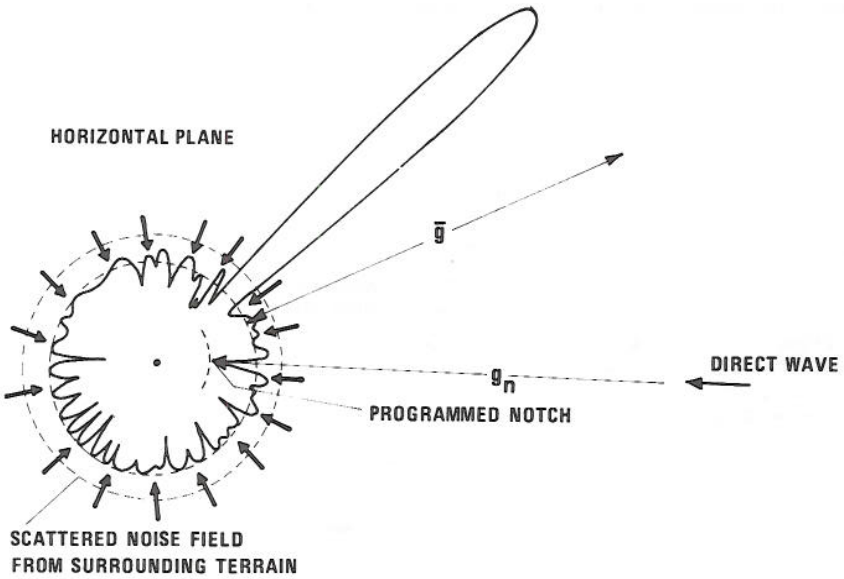

Figure 6.2 Illustration of ground scattered noise energy into the antenna side lobes and direct reception through a programmed notch

The received jamming noise power directly through the notch is given by

$$N = \frac{\sigma \, BG \, \lambda^2 \, g_n}{(4\pi \, R_j)^2 \, k}$$

where B = radar bandwidth (Hz)

g_n = notch minimum point relative to main beam max gain

k = $\Delta F/B$ = ratio between the jamming noise band ΔF and the radar bandwidth B

By equating N = KTBT, g_n is given by

$$g_n = k\frac{16\pi^2 \, kTF \, R_j^2}{\sigma \, G \, \lambda^2}$$

The highest noise density occurs under spot frequency jamming. However, spot jamming at 10 cm wavelength will normally mean a relatively narrow band of about 5 MHz. Depending upon radar bandwidth, k may vary between 1 and 50. Similarly, barrage jamming over 300 MHz leads to a k-variation between approximately 300 and 3000.

Inserting the same parameters as in equation (6.1), the relevant value for σ and estimated value for $R_j g_n$ as function of bandwidth ratio are presented in Figure 6.3.

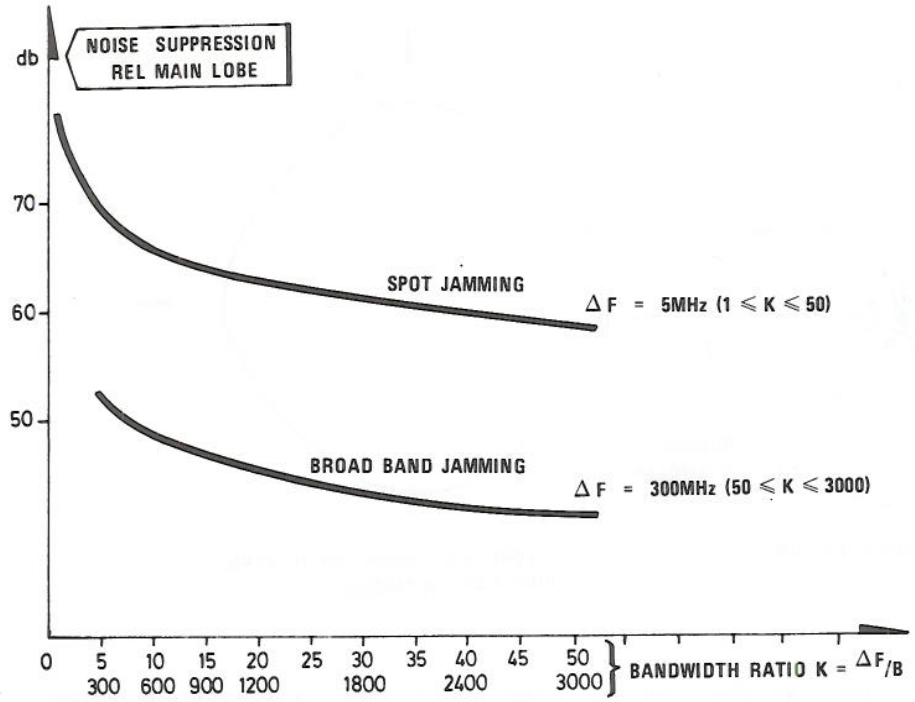

Figure 6.3 The required notch depth relative to main beam maximum gain to reduce jamming noise power to thermal noise level

The result indicates that suppression of spot noise jamming to radar thermal noise power requires a notch depth between 60–70 dB relative main lobe.

These calculations are based upon a maximum threat estimated for the next few years.

If an average side lobe level of approximately –40 dB or better is realized, it will for the time being also be assumed that the other points listed (a–d) are satisfied. This, however, must be verified through actual field measurements of a practical antenna.

6.2 Auxiliary antenna characteristics

The auxiliary antenna must be omnidirectional, but not necessarily isotropic. Nulls in the diagrams cannot be accepted since the antenna in that particular direction is obviously not able to produce any cancellation vector.

A possible auxiliary antenna design is shown schematically in Figure 6.4.

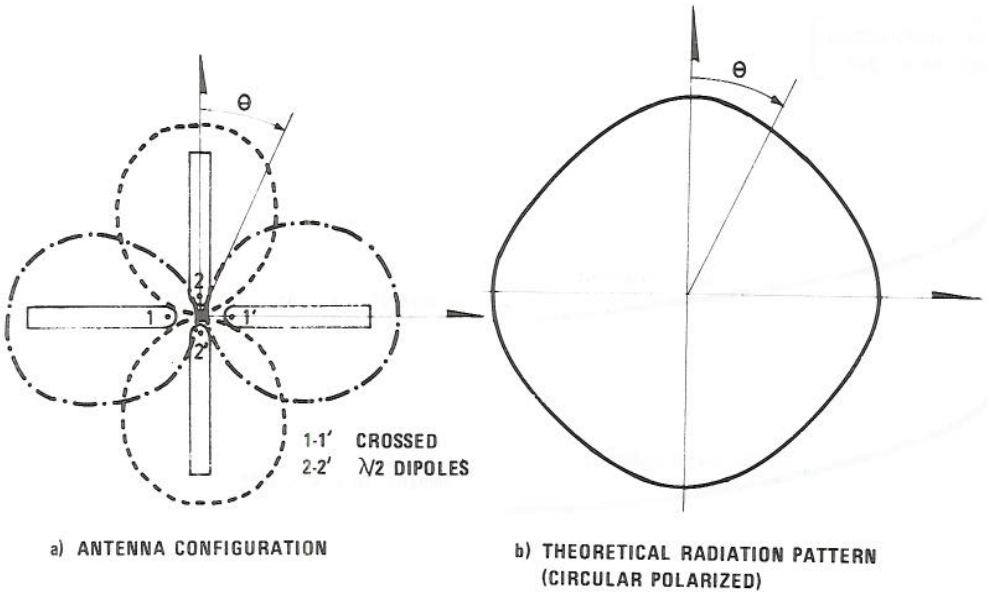

Figure 6.4 A possible auxiliary antenna design and its theoretical radiation pattern

Two crossed λ/2-wave dipoles in the horizontal plane are fed in phase quadrature. The received output signals from both dipoles are added independently through a hybrid network.

The combined output signal y(t), assuming a dipole cosine radiation diagram, is then given by

$$\begin{aligned} y(t) &= \cos\theta \ \cos wt + \sin\theta \cos(wt - \pi/2) \\ &= \cos(wt + \theta) \end{aligned} \qquad (6.4)$$

Equation (6.4) gives an ideal isotropic radiator. However, since the λ/2-wave dipole pattern is closer to a $\cos^2$-radiator the theoretical radiation diagram deviated from an ideal circular pattern by approximately 5% as illustrated in Figure 6.4b.

A test antenna and the measured radiation diagram in azimuth and elevation are shown in Figure 6.5.

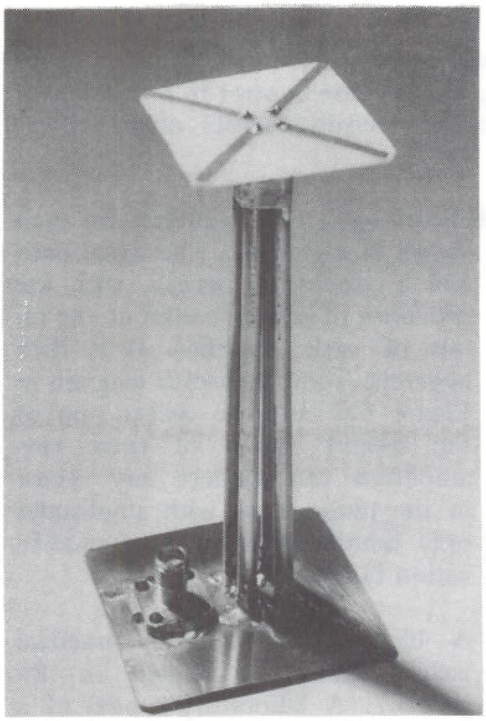

a) TOP VIEW OF CROSSED DIPOL

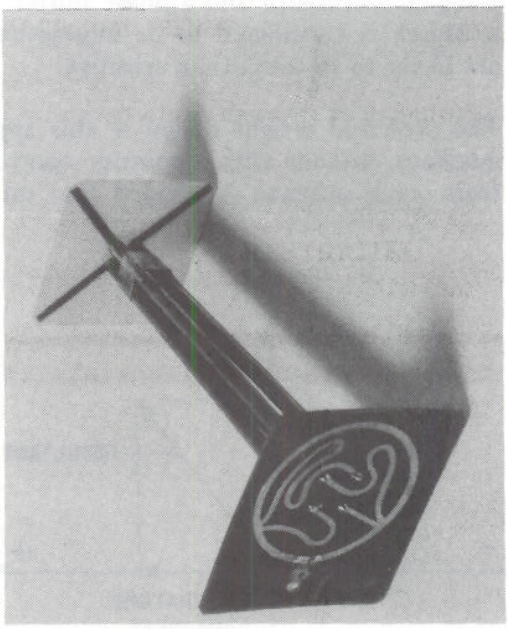

b) BOTTOM VIEW SHOWING HYBRID RING FEEDER

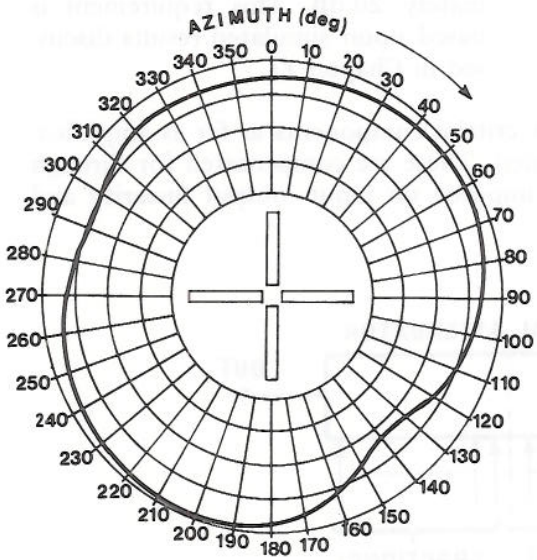

c) RADIATION PATTERN IN THE HORIZONTAL PLANE f=3.15 GHz

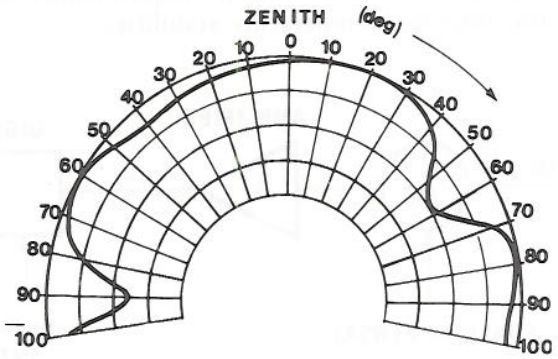

d) RADIATION PATTERN IN THE ELEVATION PLANE. THE DIPS D_1 AND D_2 ARE CAUSED BY THE COAXIAL FEEDER

Figure 6.5 An experimental antenna and its measured radiation diagram in azimuth and elevation
VSWR $\leqslant$ 1,2 at f = 3,156 GHz

6.3 The weight design

The most direct way to design the weights is to use an ordinary amplifier followed by a digital attenuator and a phase shifter. However, direct phase control to a fraction of a degree is considered to be impractical at 10 cm wavelength. Besides, phase shifters are likely to be amplitude sensitive.

The preferred weight design in this application is based upon two amplifiers for each auxiliary antenna with amplitude control only as shown in Figure 3.2. The signal path from each antenna is divided into an *in-phase* and a *quadrature* branch, with the provision of phase reversal at the input of each amplifier. It is then apparent from the vector diagram in Figure 6.6 that the vector sum of the output signals of these two amplifiers can produce any vector in the phase plane with amplitudes only limited by the weight amplification factor.

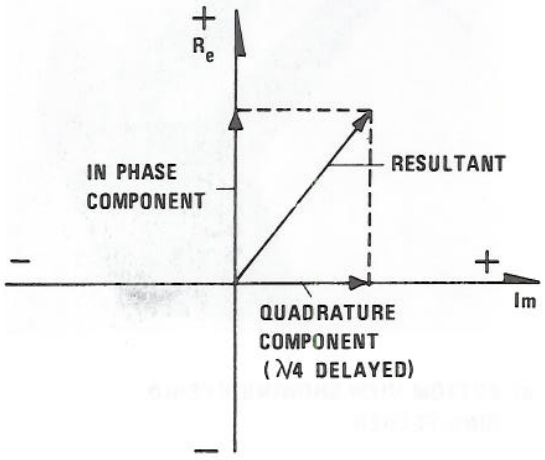

Figure 6.6 Phase and amplitude control by vector addition

A block diagram of a practical weight design is shown in Figure 6.7. A laboratory model of a test amplifier with gain, bandwidth and linearity is shown in Figure 6.8.

The net amplification required, with attenuator set to zero, including attenuator insertion loss, is approximately 20 dB. This requirement is based upon simulated results discussed in Chapter 11.

As already pointed out, the amplifiers are not critical components as far as amplification factor and static phase shifts are concerned. These are compensated for through calibration. More stringent requirements are imposed on input–output linearity and the amplifier temperature stabilities.

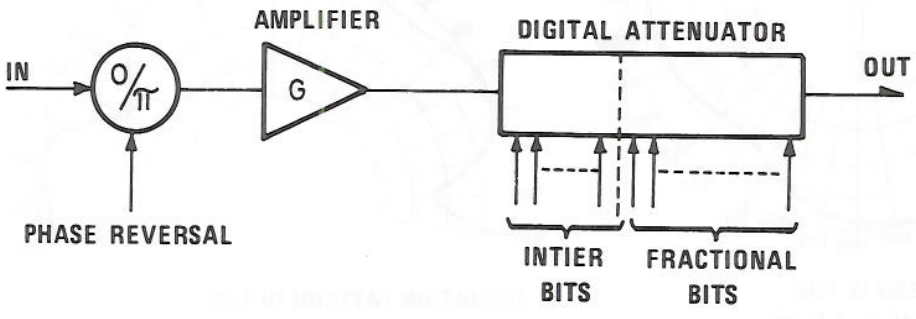

Figure 6.7 Principle of weight design

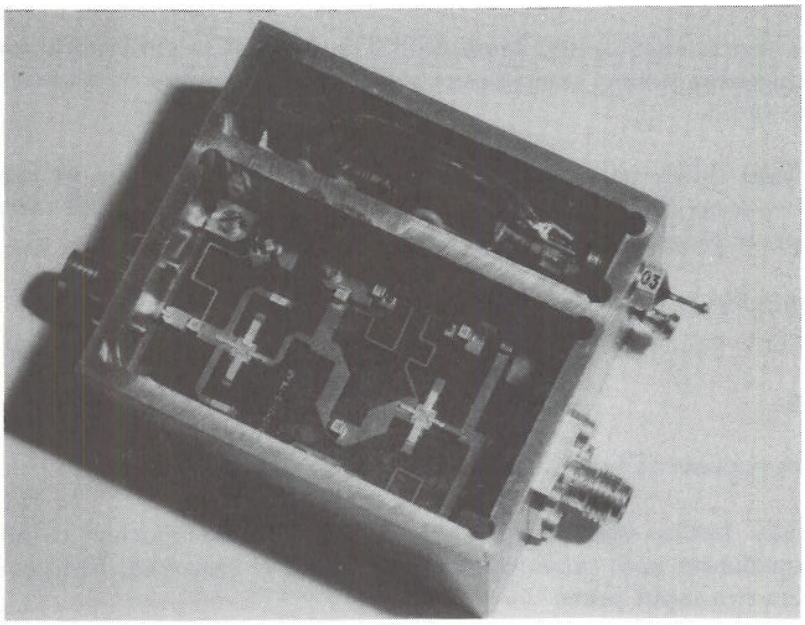

a)

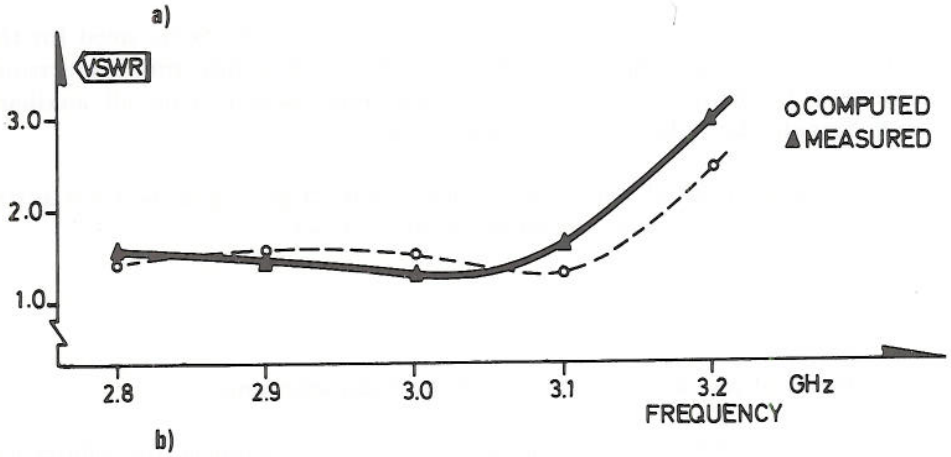

b)

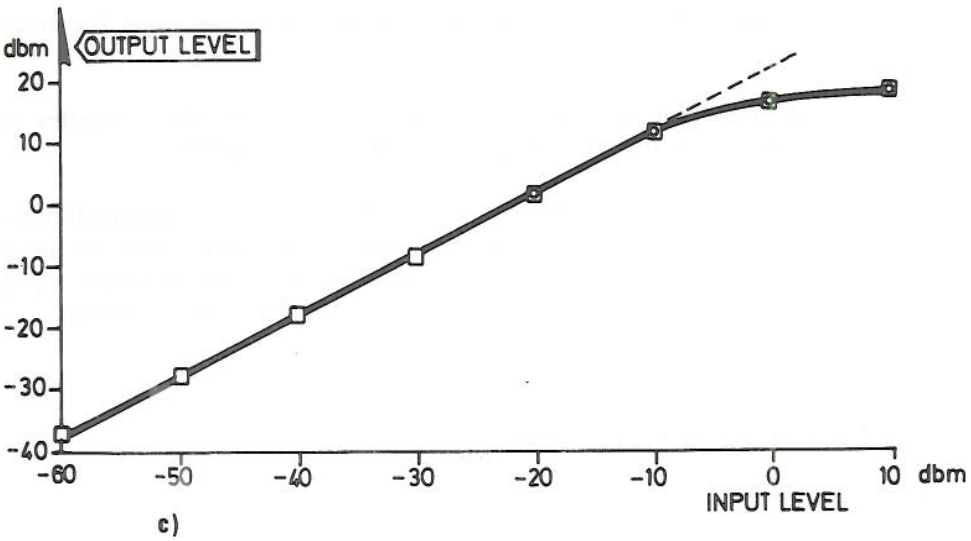

c)

Figure 6.8 An experimental S-band amplifier
a) circuit layout
b) input voltage standing wave ratio (VSWP)
c) amplifier linearity and gain

Regarding attenuator characteristics, the most critical requirements are input-to-output phase shift *vs* attenuator setting, temperature stability, repeatability of attenuator settings and switching speed.

Small variations in phase shifts, temperature variations and repeatability can be taken care of by the adaptive loop directly. Greater variations must be recorded and corrected for through computer programming.

Required switching speed is in the order of 1 μs.

6.4 The summing network

The summing network consists of hybrid rings as illustrated in Figure 6.9.

Hybrid rings are nearly lossless and ideal adders. They are easily matched to 50 Ω input and output impedances and, provided reasonable care is exercised, little coupling exists between the two input ports.

Under quiet conditions, with no interfering sources present, there is no need for the auxiliary antennas. In this case input port No 1 of the tenth hybrid ring is electronically short-circuited to ground. Otherwise, thermal noise power from all auxiliary antennas would degrade the radar receiver noise factor.

Since the hybrid ring is matched and nearly lossless, the target signal will not suffer any appreciable degradation by short-circuiting input port No 1.

6.5 The computer

The computer consists of an electronic store and an arithmetic unit.

The size of the store depends upon the number of auxiliary channels, the calibration resolution angle (solid angle increment) and the required elevation angle for which calibration must be provided.

The arithmetic unit receives direction information to the jammers and computes the required weight distribution for any incremental antenna beam position.

The computer is not a critical component in the PNS system. It is assumed that a number of general purpose types available on the commercial market may be modified and matched to this application. If extensive modifications and interface equipment are necessary, a tailor-made computer may instead prove the best solution.

7 DESCRIPTION OF THE ADAPTIVE LOOP

7.1 Principles of operation

As pointed out in Chapter 3, the programmed weight setting will establish a "null" with minima normally slightly off the direction to the interference sources. This is due to different errors which invariably are present. The purpose of the adaptive loop is to adjust the weight setting such that the noise minimum point is reached in the quickest possible way. For this purpose an algorithm based on the Steepest Decent Method is found useful.

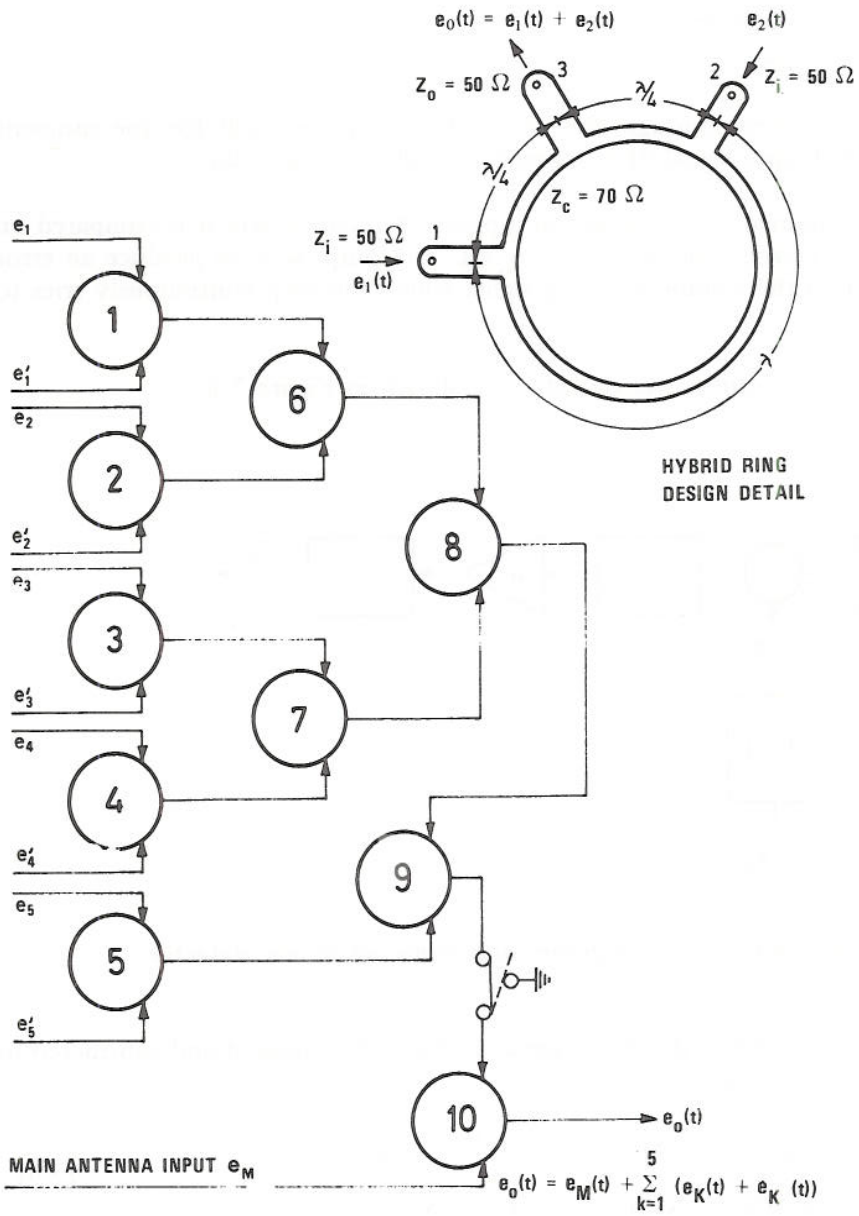

Figure 6.9 Micro strip hybrid ring summing network

The weights are designed to cover the total radar band which amounts to approximately 10% of centre frequency. The calibration system as well as the inner adaptive loop must on the other hand operate on a band matched to the radar signal bandwidth.

Following the summing network there is an RF amplifier – a mixer and then a band-limited IF-amplifier stage. The output signal y(t) will consist of

$$y(t) = N_T(t) + N_J(t) + S(t) \qquad (7.1)$$

where $N_T(t)$ = radar thermal noise
$N_J(t)$ = interference noise
$S(t)$ – desired signal

Considering noise received through the side lobes only, we will for the moment disregard a possible desired signal S(t) received through the main lobe.

The noise signal contained in y(t) is fed to a power detector where it is compared on a power basis to a reference noise source $N_R(t)$. The purpose is to produce an error signal proportional to the residue jamming signal which the loop continuously tries to reduce to zero.

The basic components of the power detector are shown in Figure 7.1.

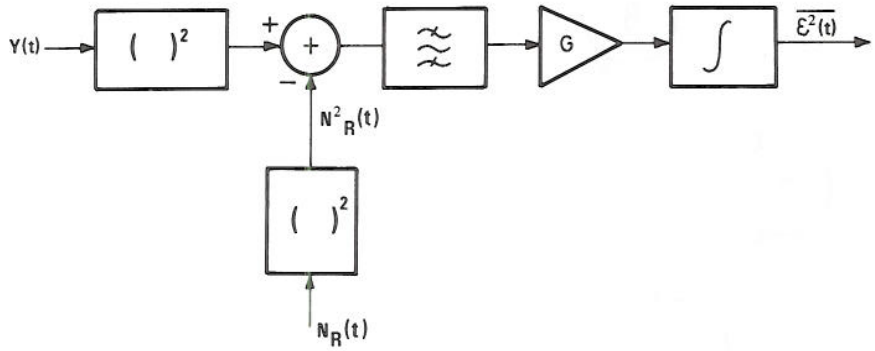

Figure 7.1 Block diagram of the adaptive loop jamming power detector

The reference signal as well as the input signal y(t) are first squared and subtracted in a summation network, giving

$$\begin{aligned} & y^2(t) - N_R^2(t) - [N_J(t) + N_T(t)]^2 - N_R^2(t) \\ & = N_J^2(t) + 2N_J(t)\, N_T(t) + N_T^2(t) - N_R^2(t) \end{aligned} \tag{7.2}$$

After band-limiting, amplification and integration, the output signal $\epsilon^2(t)$ is given by

$$\overline{\epsilon^2(t)} = G\,[\overline{N_T^2(t)} + 2\,\overline{N_J(t)\, N_T(t)} + \overline{N_T^2(t)} - \overline{N_R^2(t)}\,] \tag{7.3}$$

The jamming- and thermal noise sources $N_J(t)$ and $N_T(t)$ are assumed uncorrelated such that the average crosscorrelation product vanishes provided the integration time constant is sufficiently long.

Choosing the reference noise power term $\overline{N_R^2(t)}$ equal to the radar thermal noise power $\overline{N_T^2(t)}$ at that point in the receiver chain, equation (6.6) reduces to

$$\overline{\epsilon^2(t)} = G\,\overline{N_J^2(t)} = P_o \tag{7.4}$$

Equation (6.7) shows that the error signal $\epsilon^2(t)$ is directly proportional to the average jamming noise power $N_j^2(t)$.

The quantity P_0 is digitized in an A/D converter and fed into a processor where the adaptive loop algorithm is executed.

7.2 The Steepest Descent Algorithm (SDA)

The basic operation of SDA is as follows:

When the programmed weights W_0 have been set the gradient

$$\nabla P_0 = \Delta P_0/\Delta W \tag{7.5}$$

is being determined.

The gradient ∇P_0 is found by measuring the output power change ΔP as function of an incremental change of the weight W_i. All weights are given the same incremental change in time sequence. Mathematically, this can be expressed as

$$\nabla P_0 = (\Delta P_1, \Delta P_2, \ldots\ldots \Delta P_i, \ldots\ldots \Delta P_n) \tag{7.6}$$

where

$$\begin{aligned}
\Delta P_1 &= P_0(W_0) - P_0[W_0 + (\Delta W, 0, 0, \ldots\ldots 0)] \\
\Delta P_2 &= P_0(W_0) - P_0[W_0 + (0, \Delta W_2, 0, \ldots\ldots 0)] \\
&\vdots \\
\Delta P_i &= P_0(W_0) - P_0[W_0 + (0, 0, \ldots\ldots \Delta W_i, \ldots\ldots 0)] \\
&\vdots \\
\Delta P_n &= P_0(W_0) - P_0[W_0 + (0, 0, \ldots\ldots \Delta W_n)]
\end{aligned} \tag{7.7}$$

Having determined the gradient ∇P_0, a new weight distribution is set according to the following equation

$$W = W_0 + k\nabla P_0 \tag{7.8}$$

The change in the weight setting is proportional to the gradient multiplied by a factor k.

If P_0 is plotted as a function of k, the curve most certainly will pass a minimum point and thereafter increase again. This curve may be approximated by a second order equation such as a parabola, uniquely determined by three points on the curve. Apart from k=0, which is already measured, $k=K_1$ and $k=2K_1$ are substituted into equation (7.8). The corresponding weights are set accordingly and the output power P_1 and P_2 measured. Now $k = K_{m1}$, corresponding to the minimum point on the parabola, is calculated, substituted into equation (7.8) and the corresponding weight distribution calculated and set.

This completes the first adaption or iteration.

The weight distribution given by

$$W_1 = W_0 + K_{m1} \nabla P_0 \tag{7.9}$$

does by no means represent the optimum weight distribution for noise cancellation. The next step is now to start with the output power P_{m1} and repeat the procedure above. The new weight distribution given by

$$W_2 = W_1 + K_{m2} \nabla P_{m1} \tag{7.10}$$

is then set, resulting in an additional noise power reduction (to P_{m2}). This completes the second iteration.

This process goes on continuously. As will be shown in Chapter 11, very few iterations are required to reach an approximate optimum weight distribution.

The algorithm is illustrated in Figure 7.2.

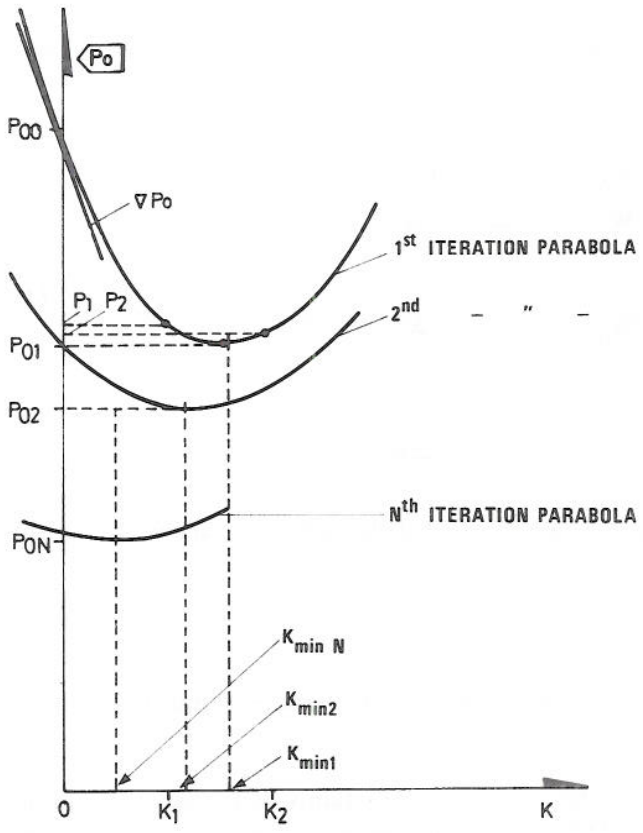

Figure 7.2 Illustration of the adaptive loop noise suppression algorithm

When the antenna has moved into the next angle resolution cell $\Delta\gamma$, new programmed weights are set and the adaptive iteration loop again starts from the beginning.

In some 3D phase scanned radar systems the antenna moves one step in elevation at the end of each transmitted pulse. Programmed weights are therefore set shortly before the radar pulse is transmitted and the iteration process starts at the moment the radar receiver is opened for reception.

8 DATA STORE REQUIREMENTS

The required size of the electronic data store is dependent upon the following factors:

- the total air volume defined by the solid angle, $r = 360°\theta$ for which programmed weights are stored.
- the notch width $\Delta\gamma$ defined at a predetermined level relative to the main lobe maximum gain. In section 6.1 this level was estimated to be approximately –60 dB.
- number of auxiliary antennas.

Practical 3D search radar antennas are normally of the separable type. Theoretically, this means that the side lobe levels in the four quadrants are given by the product of the corresponding side lobe levels on the main axis. This is illustrated in Figure 8.1. It will be observed that the side lobes outside $\pm\theta/2$ and $\pm\alpha/2$ are below the –60 dB limit as previously discussed. There is, therefore, no need to record and store data outside the angle θ and α. In practice, snow, ice, rain and temperature variations will increase the side lobe levels also in the quadrants, but presumably not more than a jammer in these regions can be suppressed by the action of the inner adaptive loop.

Stand-off jammers (SOJ) are expensive and vulnerable aircraft. They, therefore, operate at long distances and rarely at altitudes higher than approximately 30 000 feet. The elevation angle to these interference sources is consequently low.

Assuming that the elevation angle to a jammer is less or equal to $+\theta/2$, the number of solid angle increments for which weight values have to be recorded and stored is approximately given by

$$N_W \sim \frac{360°\theta - \Delta\theta\cdot\Delta\alpha}{(\Delta\gamma)^2} \qquad (8.1)$$

where $\Delta\gamma$ is the notch width in both azimuth and elevation as illustrated in Figur 8.2.

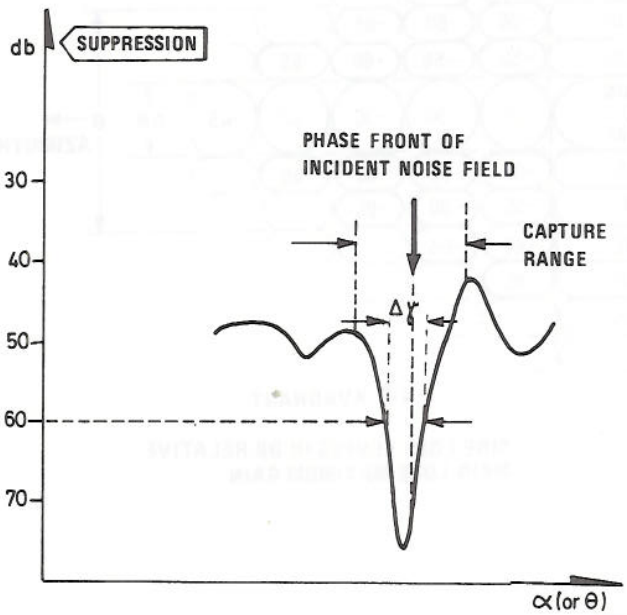

Figure 8.2 Definition of notch width

Simulations have shown (Chapter 11) that more than 80% of the notches under simulated conditions are within 0.3° at –60 dB level. Based on these results it has been concluded that $\Delta\gamma = 0.3°$ may be a good choice.

Assuming five auxiliary antennas (10 weights) the required store capacity as function of the belt width θ is shown in Figure 8.3.

The minimum requirement would be to store the calibrated weight values only (Curve A). However, when more than one jammer is present the weight distribution has to be

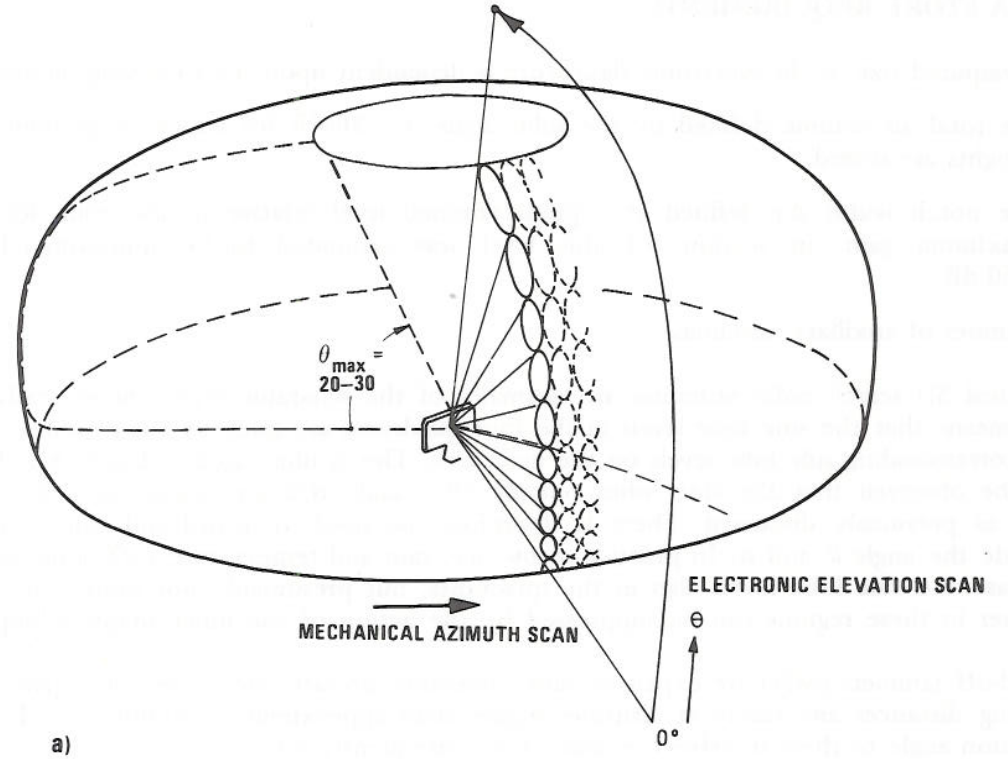

a)

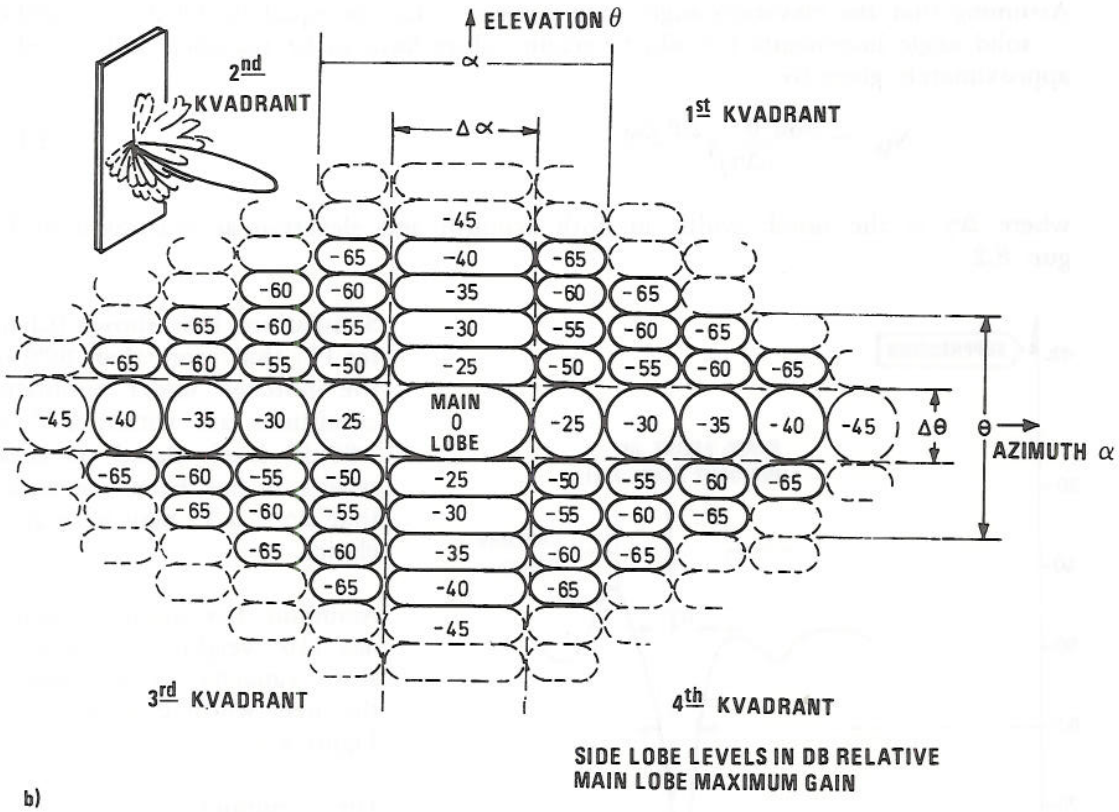

b)

Figure 8.1 Pictorial representation of
a) the antenna scan pattern
b) the relative side lobe level

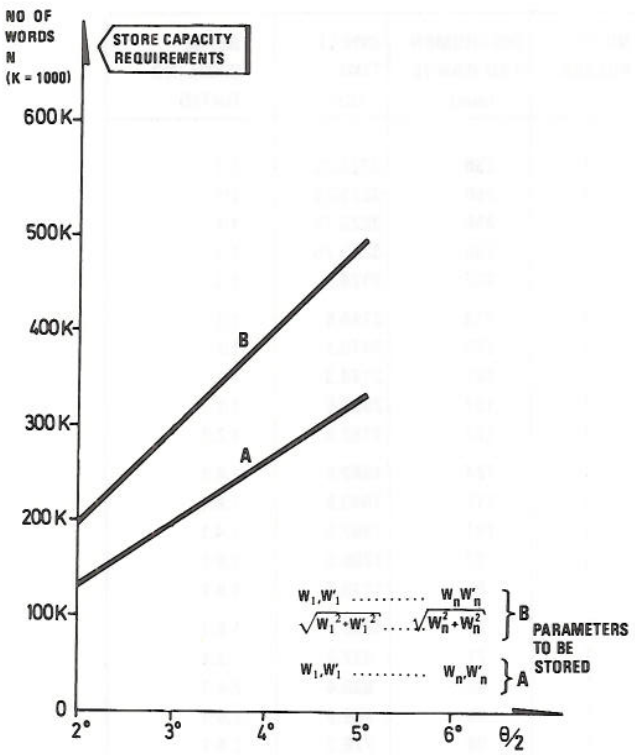

Figure 8.3 Store capacity requirement as function of belt width θ (one discrete frequency)

calculated, which involves solving trigonometric functions. To reduce the time required to solve the linear equation it would, therefore, be convenient to calculate and store the quantity $\sqrt{W_{ij}^2 + W_{ij}^{2\,1}}$ as well.

This leads to the store capacity requirement shown by curve B in Figure 8.3.

The width θ and α around the main axis where the side lobes are relatively high depends on the antenna construction and the aperture illumination function. Based on practical antenna design, it is estimated that the belt width θ including side lobes higher than −50 dB would be less than 10°.

9 THE CALIBRATION SYSTEM

Apart from its prime function of providing a noise source for calibration, the simulator is also intended to be used for performance tests of the PNS system. In fact, the system would know no difference between the simulator and a real distant jammer.

The physical arrangement of the calibration system depends on radar antenna size, beam width and its elevation scanning pattern. In this chapter it is shown how calibration can be carried out for a typical modern 3D land-based search radar system.

Typical antenna data and beam scanning characteristics are shown in Table 9.1.

It appears that the first step in elevation covers 0.6°, the next 0.75° and from then on the average step is approximately 0.9° up to the tenth beam position.

Again, the requirement is to calibrate in elevation as well as azimuth at intervals of 0.3° up to a maximum elevation of 5°.

A sketch of one possible physical configuration of the calibration system is shown in Figure 9.1. At the top of a mast positioned at a distance R from the main radar antenna, three low gain antennas are mounted above each other. The angle between two adjacent antennas as seen from the radar phase centre is approximately 0.3°. The mast height H is such that the angle between the horizontal line and the top antenna 1 is half the belt width θ as defined in chapter 8.

BEAM NO	ELEVATION ANGLE (deg)	STACK FACTOR	PULSE WIDTH τ (μs)	NO OF PULSES	INSTRUMENTED RANGE (nmi)	DWELL TIME* (μs)	BEAM SPOILING RATIO	
1	0.1	1.7	100	1	250	3223.75	1:1	
2	0.7	1.4	100	1	250	3223.75	1:1	
3	1.5	1.3	100	1	250	3223.75	1:1	
4	2.4	1.3	100	1	250	3223.75	1:1	
5	3.2	1.3	100	1	242	3124.9	1:1	
6	4.1	1.2	100	1	213	2766.6	1:1	
7	4.9	1.2	100	1	189	2470.1	1:1	
8	5.9	1.2	100	1	167	2198.3	1:1	
9	6.7	1.3	100	1	151	2000.6	1:1	
10	7.6	1.4	25	1	137	1752.6	1.2:1	
11	8.5	1.4	25	1	124	1592.0	1.4:1	
12	9.6	1.3	25	1	112	1443.8	1.4:1	
13	10.8	1.3	25	1	101	1307.9	1.4:1	
14	12.0	1.3	25	1	93	1209.0	1.4:1	
15	13.4	1.2	25	1	85	1110.2	1.6:1	
16	14.9	1.2	25	1	78	1023.7	1.6:1	
17	16.7	1.3	25	1	71	937.2	2:1	
18	18.7	1.2	25	1	63	838.4	2.4:1	
19	21.3	1.2	25	1	55	739.5	2.8:1	
20	23.8		25	1	60	776.3	2.8:1	
21	4.5	1.0	2.3	3	60	2258.9	1:1	MTI Processing
22	3.4	1.0	2.3	3	60	3000.2	1:1	
23	2.3	1.0	2.3	3	60	3000.2	1:1	
24	1.2	1.0	2.3	4	60	3000.2	1:1	
25	0.1		2.3	4	60	3000.2	1:1	

$G_T = G_R = 39.8$ dB
Beam width el = 1.1°
" " az = 1.9°

Total Elscan Time = 50.92 ms
Azimuth Stack Factor = 1.24
Average Power = 26.2 kW

*Includes 35 μs dead time for each beam (Beams 1 through 19 include an additional 1 pulse-width live time to achieve full instrumented range)

Table 9.1 Elavation beam schedule for normal surveillance with 60 NMI MTI

With the beam in the bottom position (elevation angle 0.1°) the antenna rotates one complete cycle in azimuth. During this revolution, calibration antenna 1 is excited and calibration is carried out for each auxiliary antenna at every angle increments of 0.3° in azimuth. During the next antenna rotation, beam in same position, calibration antenna 2 is excited and calibration carried out as above. At the beginning of the third rotation the radar antenna is given the first elevation step of 0.6°. During the third rotation calibration antenna 1 is again switched on, during the fourth rotation antenna 2, and so on. Table 9.2 gives the whole calibration procedure up to and included an elevation angle of 10.8°. This completes the calibration.

It will be noted that calibration in elevation is not divided into equal intervals of 0.3°. This is due to the fact that the steps in the elevation scanning are not an integer product of 0.3°. In practice one may wish to average out the increments to reduce a few but relatively large errors occurring at the beginning of the third, twelfth and thirteenth antenna position.

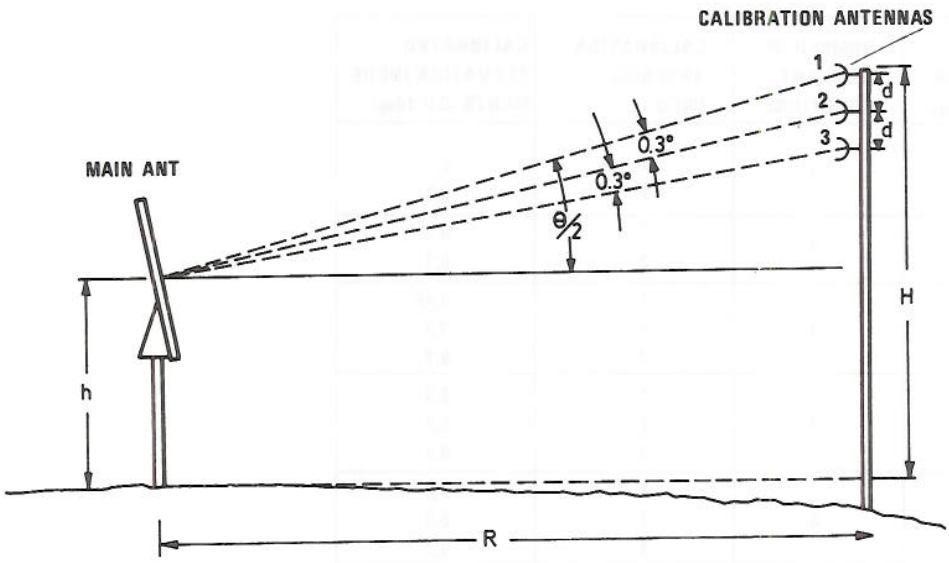

Figure 9.1 The calibration antenna system

The average value $\Delta\theta$ is given by

$$2\overline{\Delta\gamma} + 2\overline{\Delta\gamma} + 30\overline{\Delta\gamma} = (0{,}8 + 0{,}1)^\circ \qquad (9.1)$$

giving

$$\overline{\Delta\gamma} = 0.315^\circ \qquad (9.2)$$

The fact that calibration is not performed at equal intervals in elevation does not introduce significant errors.

The height of the mast is given by

$$H = h + R \tan \theta/2 \qquad (9.3)$$

and the height difference between the auxiliary antennas

$$d \sim R \tan (\Delta\gamma) \qquad (9.4)$$

By substituting:

$R = 300$ m
$\theta = 5^\circ$
$h = 5$ m
$\Delta\gamma = 0.34^\circ$

we find

$H = 18$ m
$d = 1.78$ m

To simulate a high power transmitter at 300 km, a power output of less than one watt is required provided the auxiliary antennas have 3–4 dB gain.

ANTENNA ELEVATION ANGLE (deg)	NUMBER OF MAIN ANT ROTATIONS	CALIBRATION ANTENNA USED	CALIBRATED ELEVATION INCREMENTS $\Delta\theta$ (deg)
0,1	2	1 2	0 0,3
0,7	2	1 2	0,3 0,3
1,5	3	1 2 3	0,45 0,3 0,3
2,4	3	1 2 3	0,3 0,3 0,3
3,2	3	1 2 3	0,2 0,3 0,3
4.1	3	1 2 3	0.3 0.3 0.3
4.9	3	1 2 3	0.2 0.3 0.3
5.9	3	1 2 3	0.4 0.3 0.3
6.7	3	1 2 3	0.2 0.3 0.3
7.6	3	1 2 3	0.3 0.3 0.3
8.5	3	1 2 3	0.3 0.3 9.3
9.6	3	1 2 3	0.5 0.3 0.3
10.8	3	1 2 3	0.6 0.3 0.3

Table 9.2 Calibration procedure up to an elevation angle of 10.8°

The most natural signal structure for calibration purposes is white gaussian noise. Under system performance tests, however, other waveforms may also be of interest, such as pulsed or swept noise jamming.

10 MAIN ERROR SOURCES

In this chapter are examined in some detail the main error sources. These stem from errors in direction determination, target movements, errors in calibration, frequency variations and non-ideal digital attenuators.

10.1 Errors in direction determination

Direction to an interference source is normally determined by using the amplitude characteristics of the antenna main beam. In case of a monopulse radar the zero crossing of the difference diagram would be convenient for direction determination of the received phase front.

The conventional strobing technique is based upon the amplitude characteristics and gives automatically the jammer direction. This is mechanized by recording the points on the main diagram between which the received noise field exceeds a predetermined level. The middle point, provided the main beam is symmetric, gives the direction to the noise source.

No data in strobing accuracy as function of jamming signal level are available. However, using the data for azimuth accuracy in target detection of the same radar as referred to previously (13), a representative idea of phase front direction accuracy can be obtained. Relevant random error components are given in Table 10.1.

ERROR COMPONENT	STANDARD DEVIATION (MRAD)
ENCODER QUANTIZATION	0.443
DIGITAL DATA QUANTIZATION	0.084
FREQUENCY INSTABILITY	0.013
ANTENNA TEMPERATURE QUANTIZATION	0.03
TEMPERATURE QUANTIZATION	0.029
SCINTILLATION	0.57
BORESIGHT ERROR	0.83
ENCODER ERROR	0.442
TOTAL RMS ERROR	1.19 = 0.068°

Table 10.1 Estimated RMS direction error to an interference source

It is assumed that the jamming signal level is sufficiently high to exclude errors due to thermal noise. Errors due to glint noise do not apply in this case.

The figures quoted in Table 10.1 are theoretically estimated values. It is therefore reasonable to assume that the total RMS error may be somewhat higher but is not expected to exceed 0.15°.

10.2 Errors due to target movements

Updating of jammer signal direction can only take place once per antenna revolution at intervals of typically 10 s. During this interval the jammer has changed position, resulting in direction errors of various magnitude.

Stand-off jammers are expected to operate at long distances and outside the range of potential offensive weapons. The rate of change of radius vector to the jammer is greatest when the aircraft is flying perpendicular to the line of sight between jammer and radar. In Figure 10.1 is shown the angular rate of change per antenna revolution as function of jammer range for two different jammer speeds.

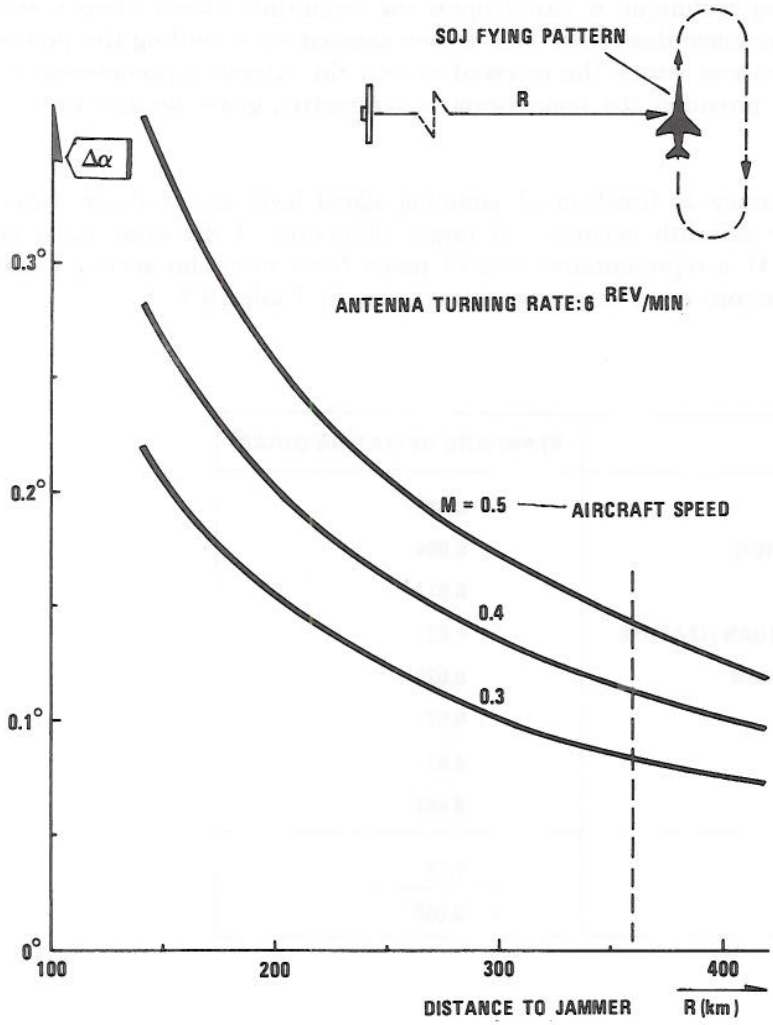

Figure 10.1 Angular change $\Delta\alpha$ per antenna revolution in the line of sight to the jammer as function of distance

As expected, appreciable angular change may occur at close ranges. This applies particularly to self-screening jammers. As for stand-off jammers, these are heavy aircraft unable to make sharp turns. In this case use of position prediction may reduce the direction error to an insignificant value.

10.3 Errors derived from calibration

Two significant errors may occur in the calibration system. One derives from the fact that the wave received from the calibration antennas at short ranges is not a plane wave. The other error is due to ground reflections.

The calibration antennas are positioned at a limited distance of 100 to 300 m from the radar antenna. This means that the received wave front over the antenna aperture is conform, as illustrated in Figure 10.2a. Compared to a plane wave the difference is that the conform wave arrival at the different antenna elements is delayed relative to the centre element by an extra path length l_n. The corresponding phase error is given by

$$\Delta\varphi_n = 2\pi\ (l_n/\lambda) \tag{10.1}$$

Assuming uniform aperture illumination the resultant output vector has a phase error $\Delta\varphi_R$ relative to a plane wave as illustrated in Figure 10.2b.

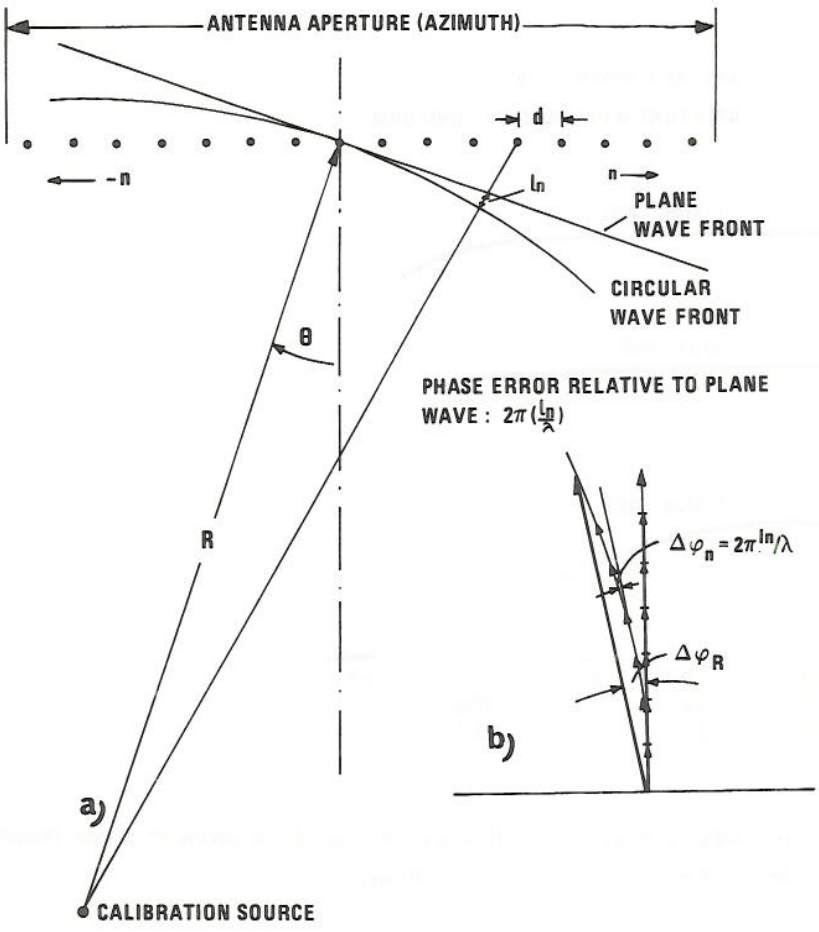

Figure 10.2 Illustration of phase error $\Delta\varphi_R$ due to conform wave front

To obtain an idea of the magnitude of the phase error, calculations have been carried out for the first, second and third side lobe of a 15 λ wide antenna aperture assuming a uniform illumination. The results are shown in Figure 10.3. The distance to the transmitter antenna is 100 m.

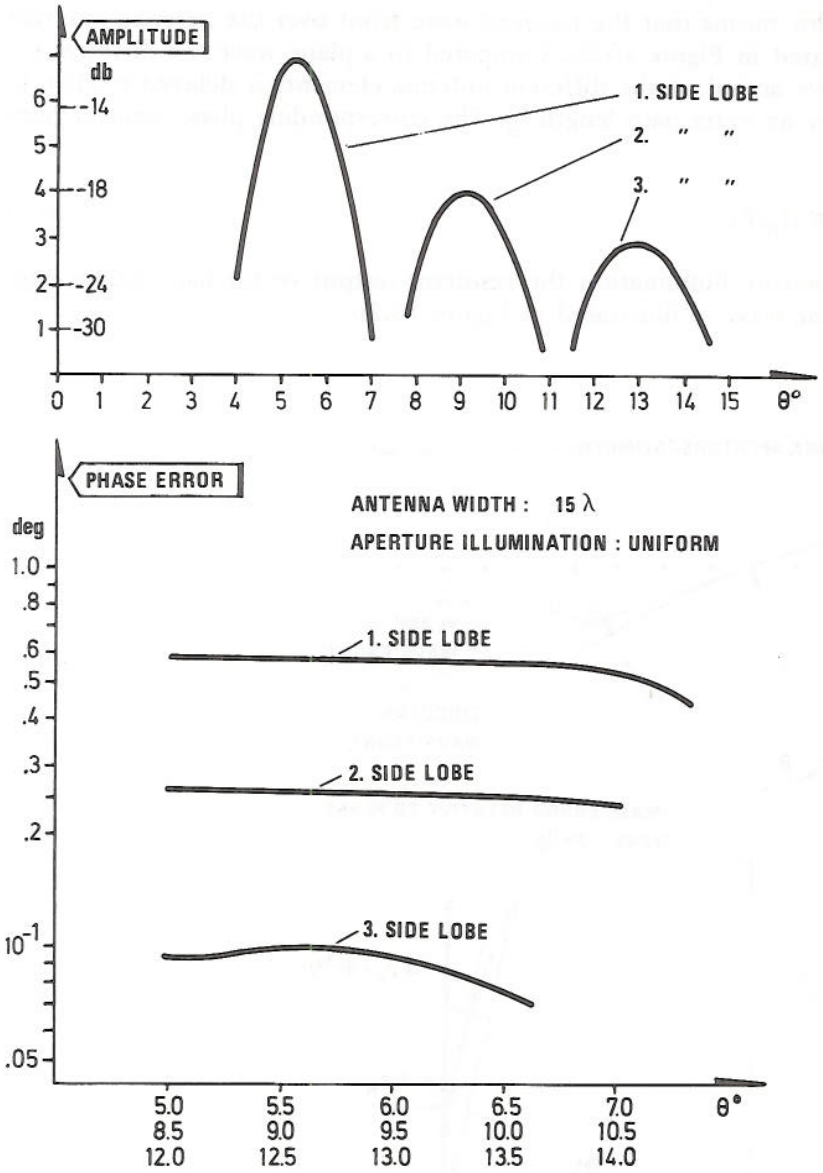

Figure 10.3 Phase error $\Delta\phi_R$ versus azimuth angle θ due to a circular wave front (distance to calibration noise source 100 m)

The computations show that a phase error of approximately 0.6° is experienced in the first side lobe. In the second and third side lobe the phase errors are, as expected, much less.

Actual antennas have much larger apertures than this simplified model. On the other hand, a tapered illumination function is normally used which tends to reduce the error contributions towards the aperture edges. It is also expected that the calibration source will be positioned at a distance of more than 100 m.

In view of these considerations and Figure 10.3, it is concluded that phase error due to conform wavefront is moderate. It should also be realized that this is a systematic error which can be corrected for by computer programming, if necessary.

10.4 Errors derived from ground reflections

Specular ground reflections from the calibration source may cause direction errors since the observed phase front at the radar antenna is the vector sum of the direct and reflected wave.

This type of error may be minimized by careful selection of calibration antenna position. Smooth surface areas between the radar and calibration antennas, which may give rise to strong reflections, should be avoided.

This type of error is therefore dependent upon local conditions. In relatively reflection-free environment where only diffuse reflections from the surrounding terrain are present, the effect of these errors is not considered significant.

10.5 Errors due to non-ideal attenuator

One major source of amplitude and phase errors may arise from non-ideal attenuators. It has been assumed up to now that phase shifts in the attenuator are not a function of attenuator setting. In practical pin diode attenuator design it seems possible to reduce phase shifts to acceptable values at the centre frequency. However, since pin diodes contain reactive elements which are tuned out at centre frequency, large phase shifts may occur at the frequency band edges.

A typical commercial attenuator tuned to zero phase shift at 3 GHz centre frequency has at 2 GHz a phase shift of 1.25 °/dB lagging and 1.25 °/dB leading at 4 GHz. Assuming linearity, this develops a phase shift of 15° at ±150 MHz deviation at 80 dB attenuation.

These large phase shifts are of course completely unacceptable. However, since these variations are systematic and can be accurately measured they can also be corrected for.

One way of correcting phase variations is to use a controlled phase shifter as shown in Figure 10.4a. The resulting phase variations are reported to be within ±3° as illustrated in Figure 10.4b (14).

It appears that such corrections could equally well be taken care of by the computer directly. Based upon accurately recorded phase variations, a routine can be programmed which enables the computer to perform the same function as the phase shifter in Figure 10.4a. In fact, it is anticipated that more accurate phase corrections can be obtained this way.

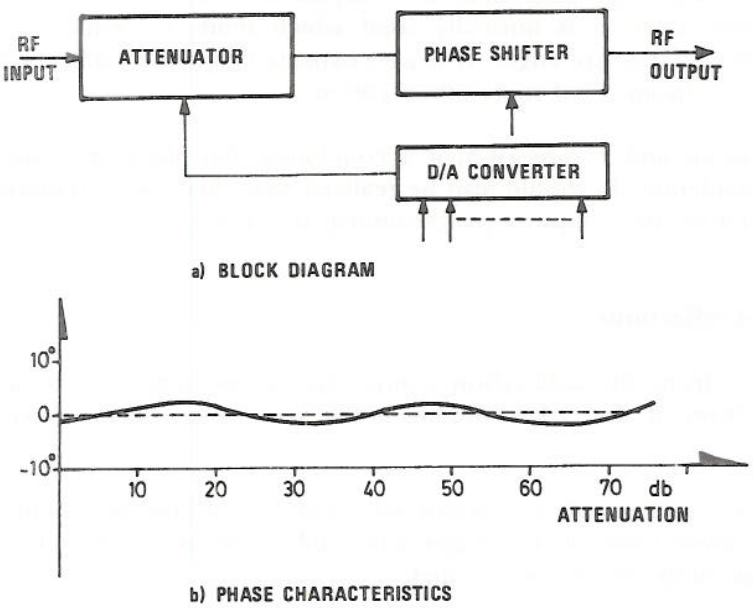

Figure 10.4 Phase controlled digital attenuator
a) block diagram
b) phase characteristics

11 RESULTS FROM SIMULATIONS

The principles of operation of Programmed Null-Steering are relatively simple compared to CSLS or ANS since it is basically an open loop system where most elements in the building blocks can be treated separately. The system is well apt for simulations which are considered a cost effective investment in the evaluation of critical parameters.

Firstly, the main and auxiliary antenna radiation diagrams must be defined. The basic radiation requirements for both antennas were discussed in section 6.1.

Two radar antenna configurations were used in the simulations, one used a 30x30 element antenna and the other a 30x60 element antenna. Both were given a Hamming illumination function and were programmed to give a maximum side lobe level of –40 dB. Also random phase and amplitude errors in the element radiators were introduced to simulate more realistic conditions. Six simulated radiation diagrams are shown in Figure 11.1 a-f.

The element antennas are assumed to be cosine radiators in azimuth and elevation according to the following relation

$$R = 0.008 + \cos \psi \qquad (11.1)$$

where ψ is defined over $0 \leqslant \psi \leqslant 180°$.

The constant 0.008 has been added to simulate a relatively high back lobe.

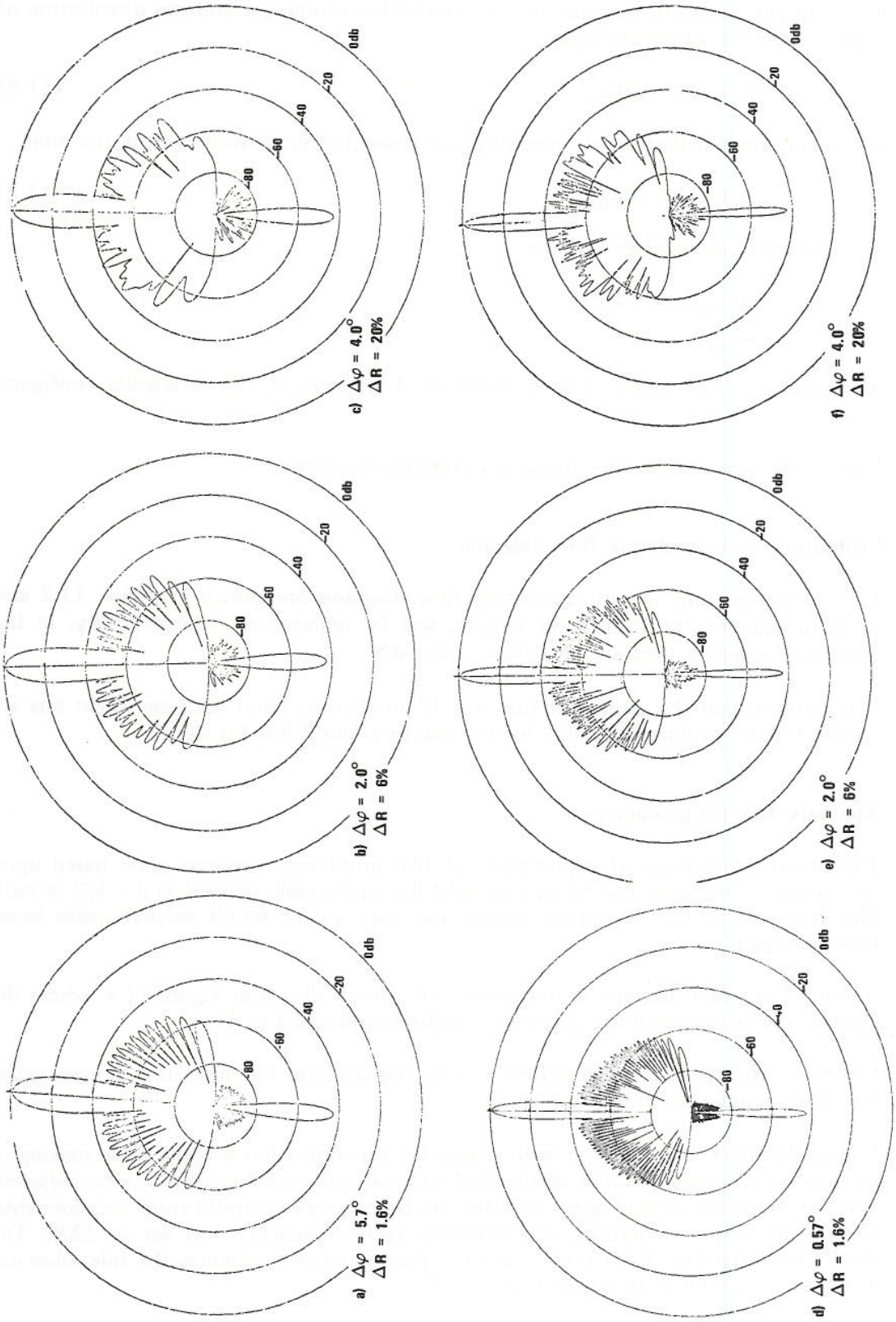

Figure 11.1 Simulated radiation pattern for different element phase and amplitude errors

a–c) 30×30 elements

d–f) 60×30 elements (60 elements in azimuth)

Errors in the radiation diagram are introduced by assuming a uniform distribution of amplitude errors within the range

$$0 \leqslant \Delta R \leqslant \Delta R_{max} \tag{11.2}$$

and a uniform distribution of received phase errors for all elements within the limit

$$0 \leqslant \Delta\varphi \leqslant \Delta\varphi_{max} \tag{11.3}$$

The maximum assumed errors were

$$\Delta R_{max} = 20\%$$
$$\Delta\varphi_{max} = 4^\circ$$

All simulations are based upon a threat of 5 jammers in various angular configurations.

Unless otherwise stated, spot frequency jamming is assumed.

11.1 Calibration- and simulation flow diagrams

The calibration and weight calculation flow diagrams are shown in Figure 11.2 and 11.3. In practice the calibration weights will be determined experimentally. In the simulation program they are, of course, calculated.

It is assumed that the arithmetic unit is a 32-bit floating point machine. Eight bits are chosen for the exponent, 22 bits for the mantissa and 2 bits for signs.

11.2 Auxiliary antenna geometry

The initial simulations of suppression of five interference sources were based upon five auxiliary antennas placed on a straight line and equally spaced at $d = \lambda/2$ (π rad). The requirement for minimum attenuation was set to 60 dB relative main beam maximum gain.

A typical antenna diagram at one instant of time is shown in Figure 11.4, where the angular spacing between the jammers is uniform and equal to 6°.

Evidently, the radar antenna suffers serious degradation. The distortion is even worse for closer angular spacing of the jammers.

It soon became clear that the main reason for this distortion was the close spacing of the auxiliary antennas. Close spacing led to small phase differences between adjacent antenna elements which again resulted in large weight amplification requirements. After some experimentation, the auxiliary antenna spacing was set to $5\lambda/2$. The results were striking. Even for 1° angular spacing between jammers the side lobes did not exceed –20 dB as shown in Figure 11.5.

The simulations continued for $d = 5\lambda/2$ at jammer angular spacings of 15°. Of a total of 1000 increments 22 cases failed to give satisfactory attenuation. In fact, singular points appeared quite frequently, to the effect that satisfactory solutions of the equations were not obtained.

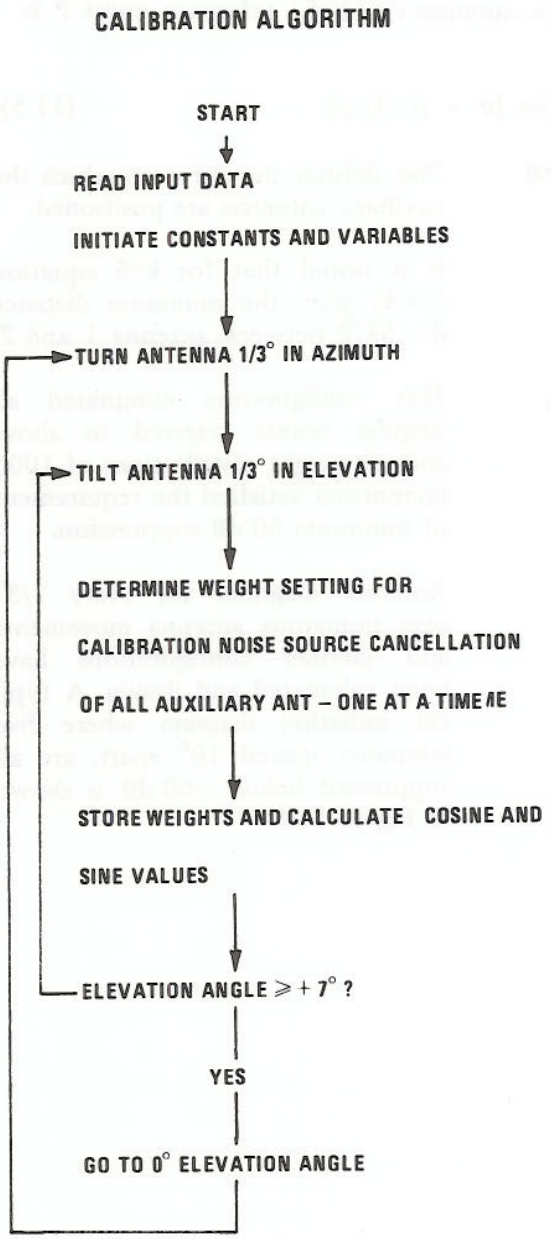

Figure 11.2 Calibration flow diagram

Examination of the antenna configurations revealed that these singular points were due to two different conditions, illustrated in Figure 11.6 a,b.

Considering two jammers only it appears that at some instant of time (the main and auxiliary antennas are mounted on the same rotating structure) a situation will occur for which $(\varphi_2 - \varphi_1) = 2\pi$. In this case

$$\begin{aligned} \sin \varphi_1 &\sim \sin \varphi_2 \\ \cos \varphi_1 &\sim \cos \varphi_2 \\ \sin 2\varphi_1 &\sim \sin 2\varphi_2 \\ \cos 2\varphi_1 &\sim \cos 2\varphi_2 \\ &\text{etc} \end{aligned}$$

Consequently, two lines in the "A" matrix are nearly equal, with the result that the set of independent equations is incomplete.

This problem can simply be resolved by choosing unequal distance between the auxiliary antenna elements.

With reference to Figure 11.6b it is also clear that twice during one antenna revolution the line through the auxiliary antennas will divide the angle between two jammers in equal halves. This results in another singular point, in that

$$\begin{aligned} \sin \theta_1 &= -\sin \theta_2 \\ \cos \theta_1 &= \cos \theta_2 \end{aligned}$$

The remedy for this difficulty is to place the antennas on a curved line.

The final configuration of the auxiliary antennas used for the rest of the simulations is illustrated in Figure 11.7.

Here the distance from any antenna i to the reference point P is given by

$$(3-i)\ \pi\ (k + 0.25\ i) \qquad (11.4)$$

where k is a constant.

The jammer signal phase difference between antenna i and the reference point P is defined as

$$\Delta\varphi_i = (3-i)\ \pi\ (k + 0.25\ i)\ \sin\ [\theta + (i-3)\ \varphi] \qquad (11.5)$$

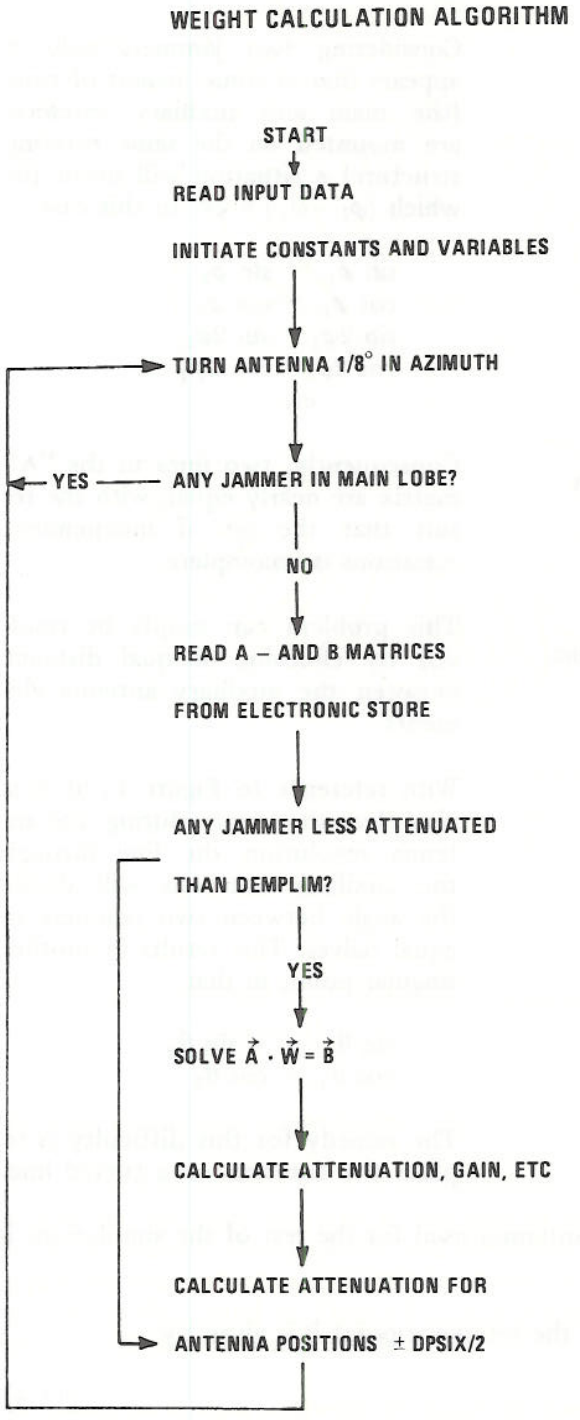

Figure 11.3 Weight calculation flow diagram

This defines the curve on which the auxiliary antennas are positioned.

It is noted that for k=5 equation (11.4) gives the minimum distance $d = 5\lambda/2$ between antenna 1 and 2.

This configuration eliminated all singular points referred to above and all weight distributions of 1000 increments satisfied the requirement of minimum 60 dB suppression.

Antenna diagrams for every 1/3° over numerous antenna movements and jammer configurations have been calculated and drawn. A typical radiation diagram where five jammers, spaced 10° apart, are all suppressed below –60 dB is shown in Figure 11.8.

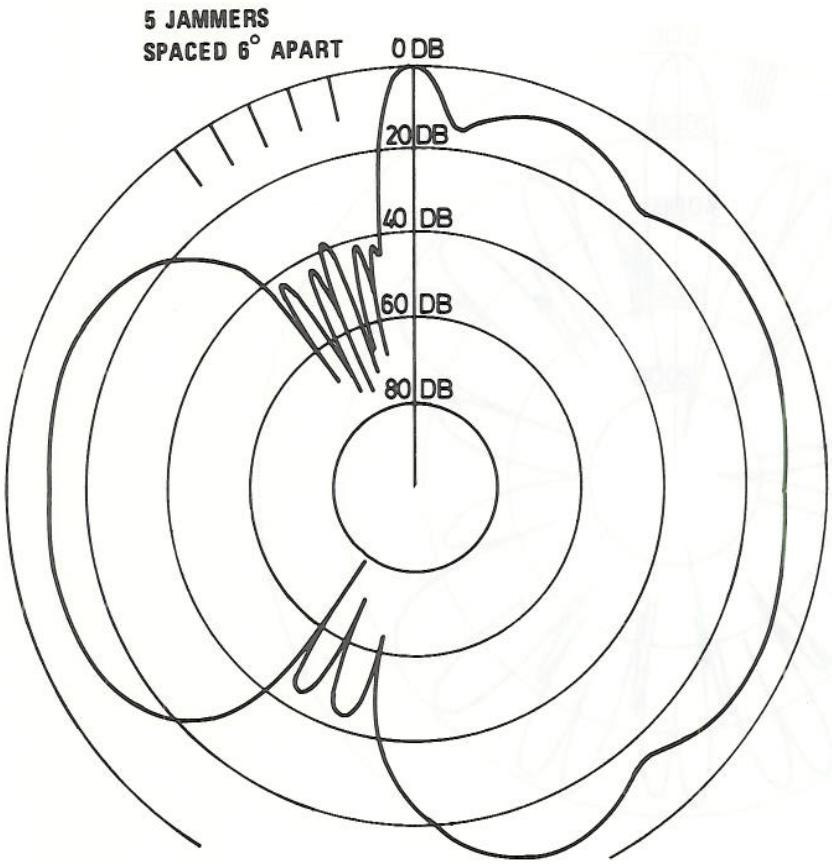

Figure 11.4 Example of main antenna radiation pattern distortion caused by close spacing of auxiliary antennas ($d = \lambda/2$)

11.3 Weight word length requirements

One parameter of primary interest is the word length requirement of the digital attenuator setting.

It is convenient to divide the total number of bits into an INTIER digital setting which in fact corresponds to the net weight amplification above 1, and a number of FRACTIONAL bits which define the limit of the quantization increments required.

All other parameters were set to such values that they would not influence the results (default values).

With the INTIER bits set to 6, which was considered well above the actual requirements, the average continuous suppression (to be defined later) was calculated as function of number of fractional bits. The result is shown in Figure 11.9a. It is evident that there is no sense in increasing the fractional bits beyond 10.

Similarly, the mean continuous attenuation was calculated as function of intier bits. The number of fractional bits was set equal to 7.

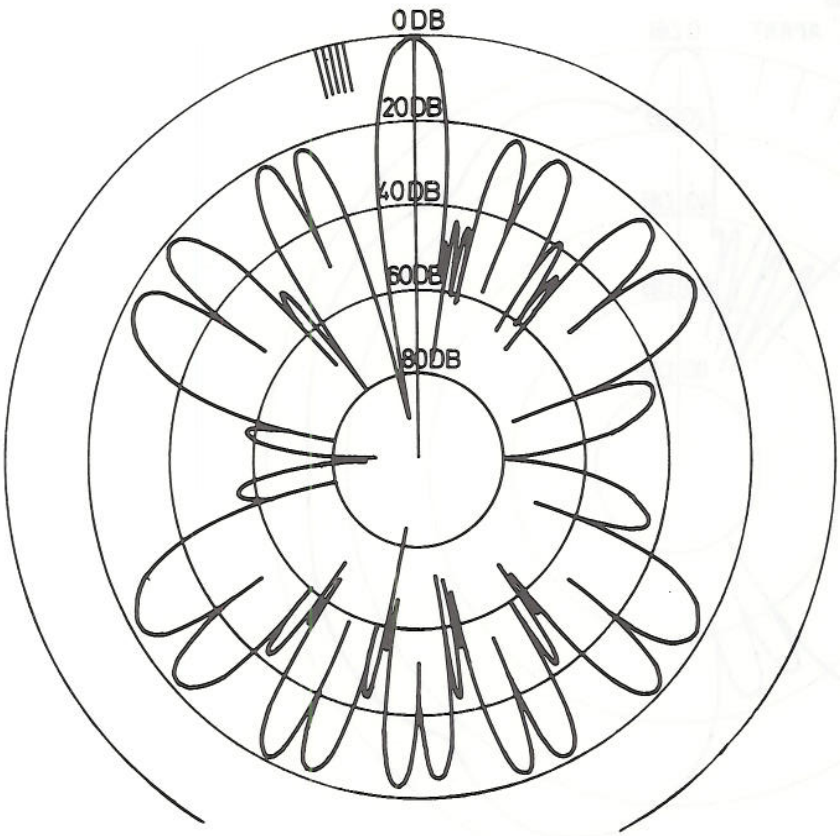

Figure 11.5 Example of main antenna radiation pattern when 5 jammers spaced 1° apart are suppressed
Auxiliary antenna spacing d = 5/2λ.

The result, shown in Figure 11.9b indicates that little is gained by increasing the number of intier bits beyond 4. (It can be argued that a greater number of fractional bits should have been chosen to ensure independence of this parameter. However, it was later proved that more fractional bits did not alter the results.)

According to Figure 11.9 a total of 4+10 = 14 bits represents an upper boundary for the bit requirement. However, a reduction to 4+7 = 11 bits will not reduce suppression more than approximately 2 dB. In view of the fact that there are also other error sources, which will tend to degrade system performance, it is concluded that the number of bits required for the weight setting will be in the vicinity of 11 bits.

Four intier bits would require a net weight amplification of 24 dB.

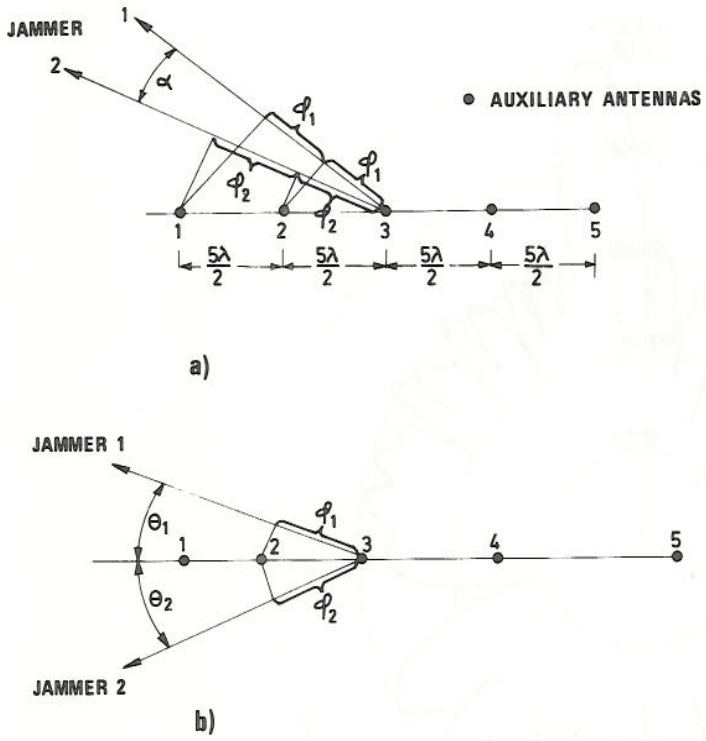

Figure 11.6 *Singular points arising from*
a) equal spacing (d)
b) straight line configuration

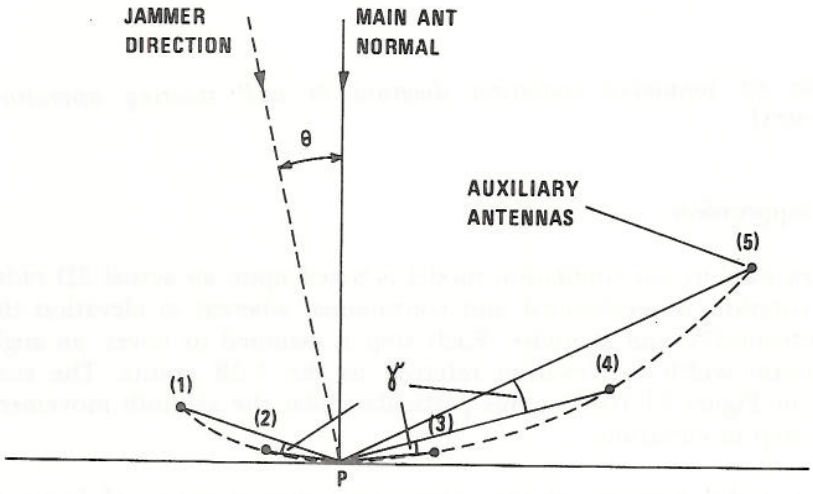

Figure 11.7 *A possible auxiliary antenna configuration*

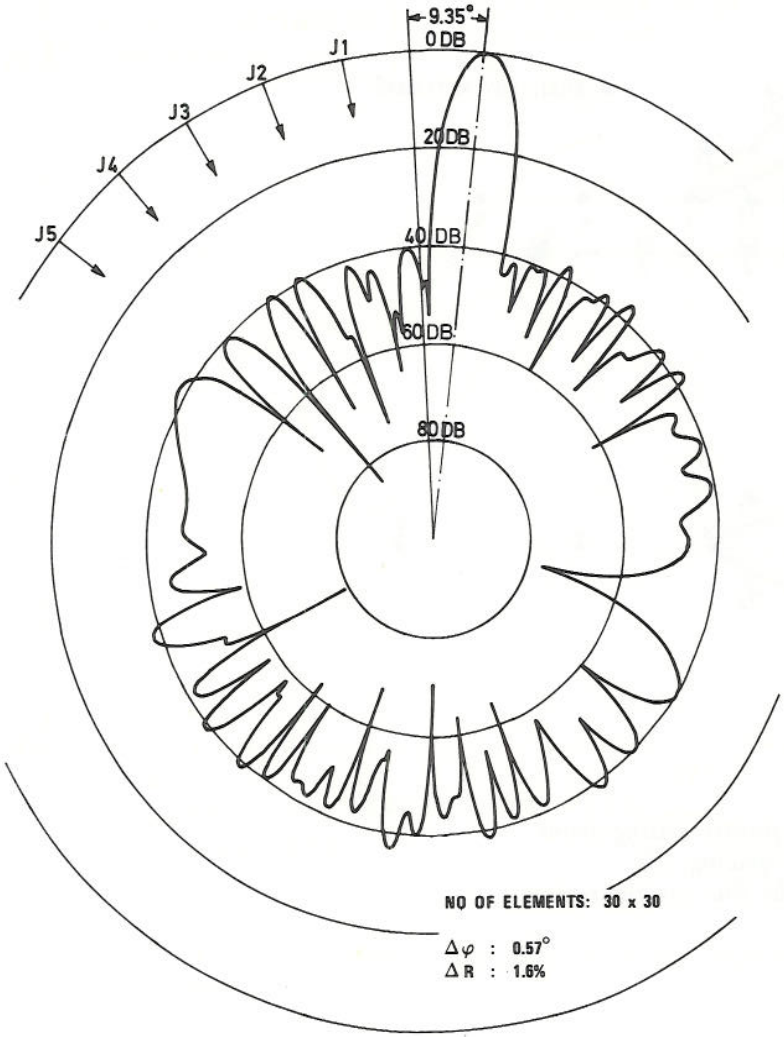

Figure 11.8 Example of simulated radiation diagram in null steering operation (5 jammers)

11.4 Average continuous suppression

The radar scan pattern used in our simulation model is based upon an actual 3D radar where the azimuth rotation is mechanical and continuous, whereas in elevation the beam is scanned electronically and stepwise. Each step is assumed to cover an angle equal to the main beam width in elevation referred to the 3 dB points. The scan pattern is illustrated in Figure 11.10. For this particular radar the azimuth movement covers 1/8° for each step in elevation.

In order to obtain a useful measure of the attenuation characteristics of jamming signals a procedure illustrated in Figure 11.11 was followed.

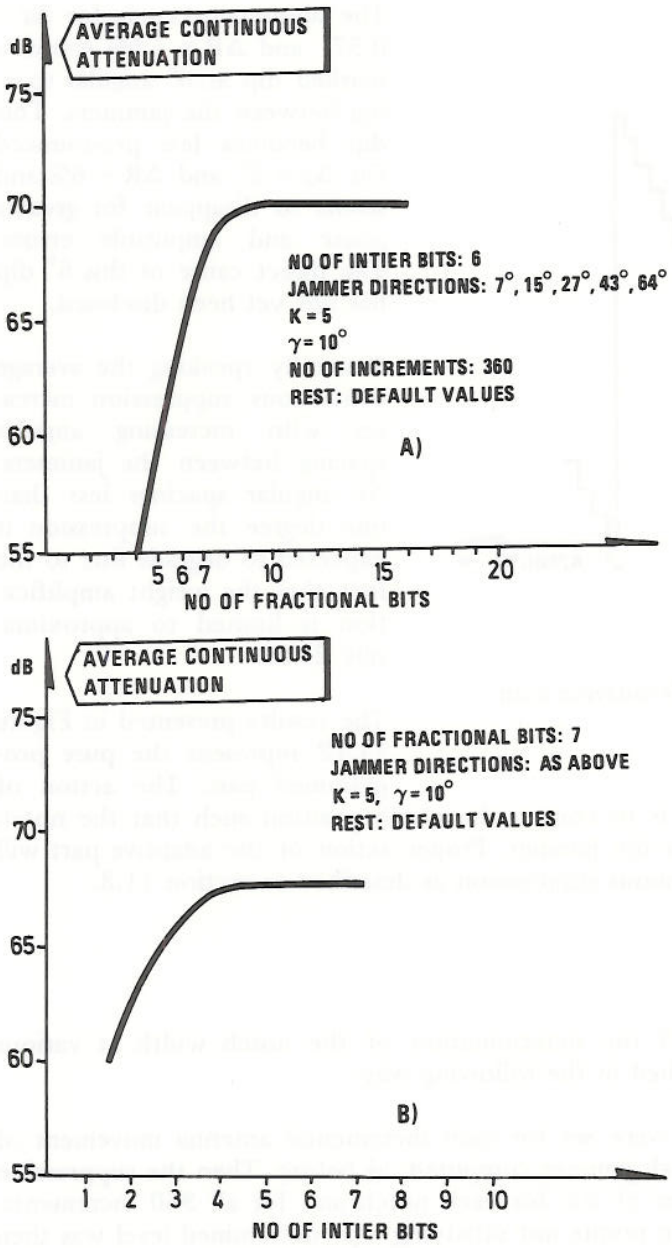

Figure 11.9 Digital attenuator word length requirements

The basic scheme is to calculate the weight distribution for a notch in the jammer direction at each 1/8°. Due to introduced errors the minimum point will normally not be in the direction to the jammer. And, as the antenna rotates, the direction to the jammer will "climb" on the notch edges and suppression (attenuation) is reduced.

The suppression is also calculated at points which lie ±1/16° to each side of the actual direction to the jammer. The mean value of the suppression obtained at these three points gives a reasonable representation of the *average suppression* over an antenna movement of 1/8°. As the antenna has completed a 1/8° movement a new weight distribution is set and the suppression is calculated at three new points on the notch curve. This is illustrated for two antenna azimuth increments in Figure 11.11.

These calculations are carried out for each jammer and for a certain number of antenna increments. The average attenuation of all jammers averaged over all antenna increments is termed the *average continuous suppression* (ACS).

In order to ensure *statistical stability* a minimum number of approximately 360 increments were found necessary. Additional sampling points beyond that number did not alter the ACS appreciably.

Numerous simulations of average continuous suppression for different jammer configurations have been carried out and given in (15). In Figure 11.12 is presented representative results of average continuous suppression as function of angular distance between the jammer for different main antenna radiation diagrams as modified by element amplitude and phase errors.

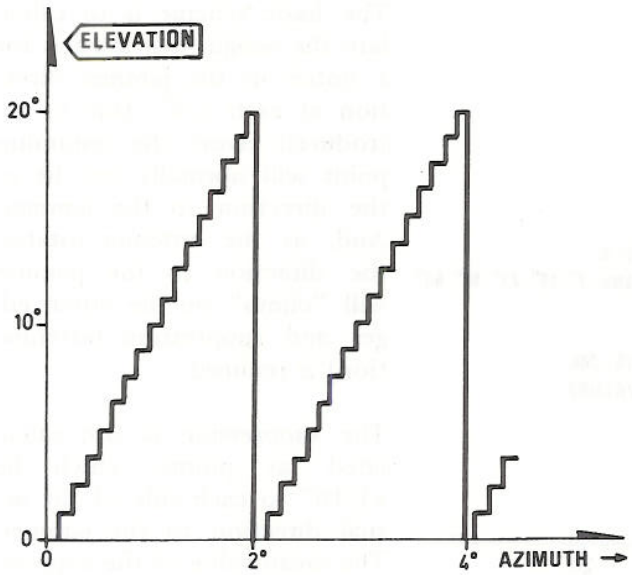

Figure 11.10 Illustration of 3D antenna scan pattern

The suppression curve for $\Delta\varphi$ = 0.57° and ΔR = 1.6% shows a marked dip at 6° angular spacing between the jammers. This dip becomes less pronounced for $\Delta\varphi$ = 2° and ΔR = 6% and seems to disappear for greater phase and amplitude errors. The direct cause of this 6° dip has not yet been disclosed.

Generally speaking the average continuous suppression increases with increasing angular spacing between the jammers. At angular spacings less than one degree the suppression is expected to degrade due to the fact that the weight amplification is limited to approximately 20 dB.

The results presented in Figure 11.12 represent the pure programmed part. The action of the inner adaptive closed loop is to correct the notch position such that the notch point is always directed towards the jammer. Proper action of the adaptive part will be to improve the average continuous suppression as described in section 11.8.

11.5 Determination of notch width

With reference to Figure 11.13 the determination of the notch width at various suppression levels was accomplished in the following way:

Computed weight distributions were set for each incremental antenna movement of 1/8° and suppression level of each jammer computed, as before. Then the suppression was computed for various values of $\Delta\psi$ for each notch and for all 360 increments. The percentage of all suppression points not satisfying a predetermined level was then determined.

The results, presented in Figure 11.14 a,b, indicate that the notch width is dependent upon the angular spacing between the jammers. At the –60 dB level 80–90% of all points are within $\Delta\psi$ = 0.3°.

The simulations indicate that new weight distributions at every 0.3° of antenna movement seem to be a reasonable choice.

11.6 Broad band noise jamming

So far we have considered monochromatic jamming signals only and assumed ideal phase coherency between received signals in the main and auxiliary channels. In practice it must be assumed that broadband and band-limited jamming signals covering the whole radar band including the image frequencies will be used. The interfering signals are therefore not a single vector but rather a vector field where full coherency between main and auxiliary channels is no longer possible. The question therefore arises as to what degree of system degradation one must expect under these conditions.

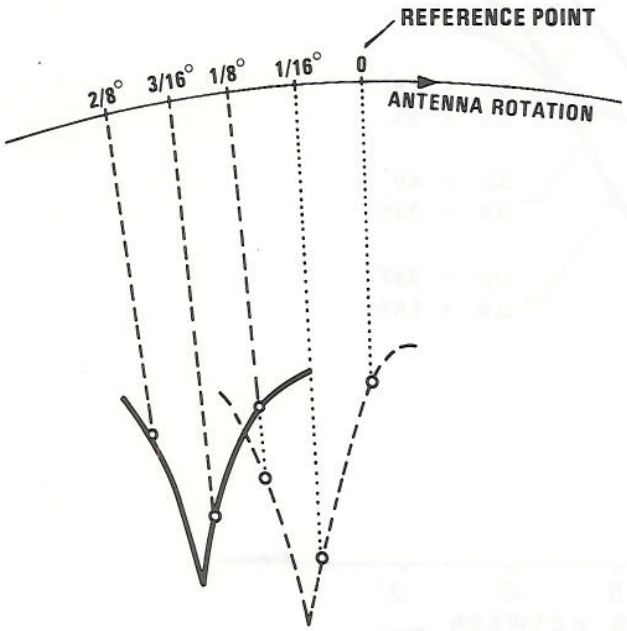

ILLUSTRATION OF TWO SUCCESSIVE NULLS

Figure 11.11 Illustration of two successive notches

Realistic simulations of band-limited jamming signals is rather complicated. However, it is possible to acquire considerable insight into the sensitivity of suppression degradation as function of frequency by calculating the suppression at different points relative to the calibrated centre frequency. To do so the associated phase error as function of frequency deviation was estimated for the auxiliary antennas, the $\lambda/4$ delay lines and for the weight and summation networks.

The results are shown in Figure 11.15 where average continuous suppression is given as function of frequency deviation and the corresponding phase error.

Although these simulations represent a simplified case, they do indicate that open loop programmed null-steering is not very sensitive to bandwidth. This is in contrast to the CSLS and ANS systems.

11.7 Simulation of the adaptive loop algorithm

In chapter 7 the procedure for additional noise cancellation through adaptive loop processing was outlined. The method was based upon repeated gradient measurements and noise level reduction using the Steepest Descent Method.

Assuming that the adaptive loop is running continuously, the time available for adaptive processing is approximately 2.4 ms. This corresponds in our radar model to the pulse repetition period and the time interval between each new antenna position. At the beginning of each new antenna position new programmed weights are set.

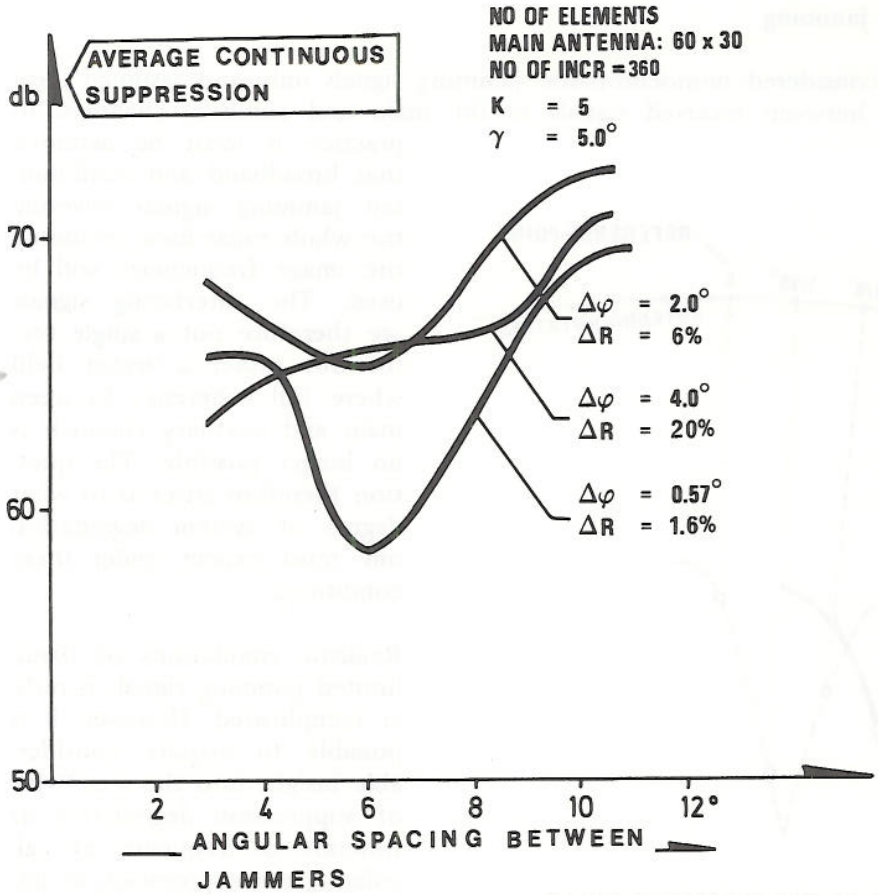

Figure 11.12 Average continuous suppression versus angular spacing between jammers

The necessary time period to make one power measurement is estimated to be $\approx 20\ \mu s$. One complete iteration, which demands 13 power output measurements (5 jammers), requires 260 μs. Hence, it is convenient to divide the time slot of 2.4 ms into 8 intervals of 300 μs each and to carry out a total of 7 iterations. No iteration will take place in the eighth interval since new programmed weights will be set at the end of this interval. Each interval of 300 μs is again divided into 15 subintervals of 20 μs. Using the same simulation model as before, the intervals and subintervals are shown in Figure 11.16.

The following steps are now carried out at every angle increment of 1/8° :

1 The programmed weights are set at the end of the eighth interval.

2 Noise power output P_{out} and attenuation are calculated at the beginning of and during subinterval 1.

3 The gradient ∇P_{out} is found by altering the weight setting by the least significant bit in all 10 weights, one at a time, during subintervals 2, 3, 4 . . . including 11. P_{out} is again calculated at the beginning of subinterval 12 and 13 using the weight distributions given by

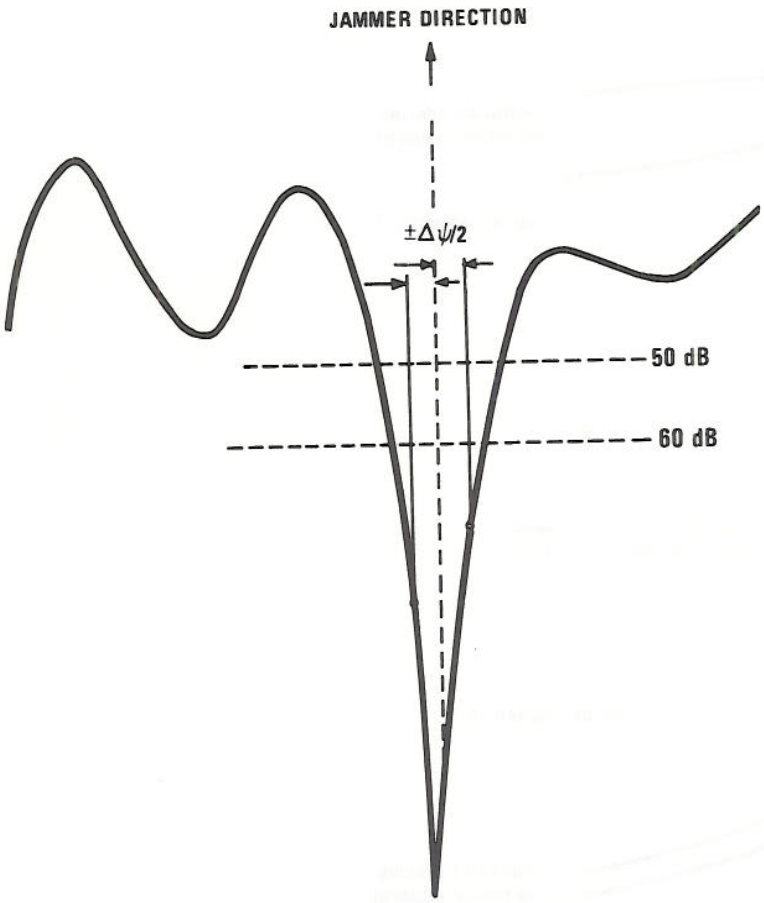

Figure 11.13 Definition of notch width

$$W' = W_n + K_1 \nabla P_{out}$$
$$W'' = W_n + 2K_1 \nabla P_{out}$$

respectively.

4 K_{min} is then calculated and the corresponding weight distribution set.

5 The attenuation at K_{min} is calculated at the beginning of subinterval 15.

6 Steps 1 through 5 are repeated for intervals 2 through 7.

During these simulations the main and auxiliary antenna gains towards each jammer were determined at every calculated value of P_{out}. The result was that the simulation time became unacceptably long. The simulations showed, however, that the antenna gain and therefore also the attenuation changed very little during an antenna movement of 1/64°. This led to a simplified algorithm consisting of the following steps:

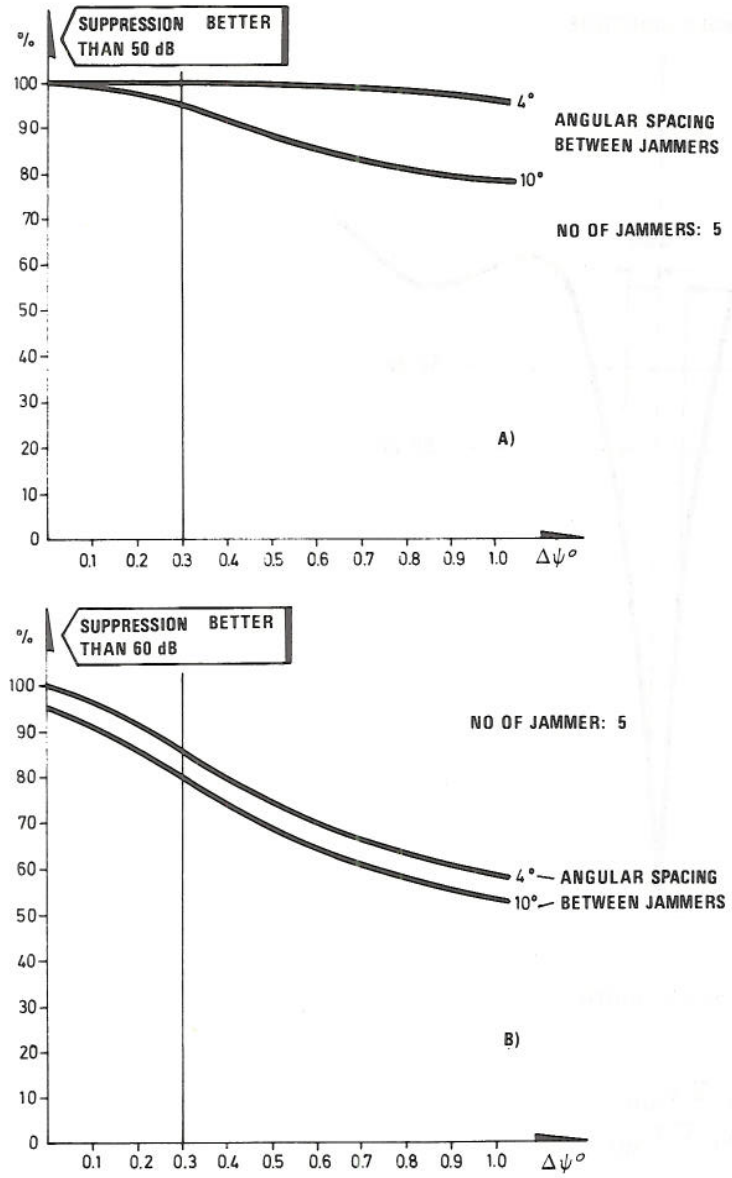

Figure 11.14 Suppression characteristics as function of incremental angle deviation $\Delta\psi$ from direction to jammer

a) percentage better than 50 dB
b) percentage better than 60 dB

1 The weight distribution calculated at the midpoint of the first interval is set at the beginning of interval 1.

2 The suppression of all jammers is calculated at the beginning of an interval.

3 The gradient is calculated and W_{n+1} is determined by referring all calculations of P_{out} to the beginning of the interval.

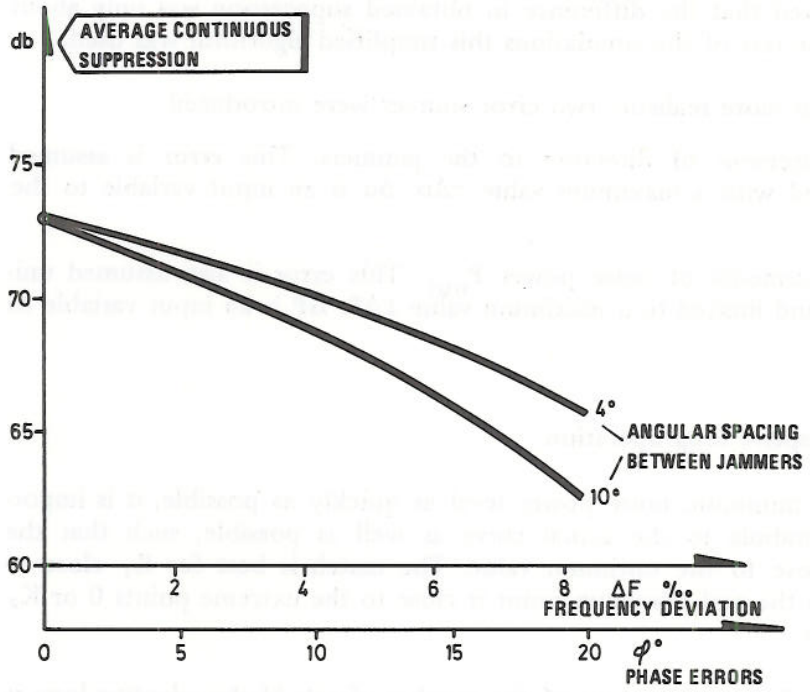

Figure 11.15 Average continuous suppression as function of frequency deviation and phase error

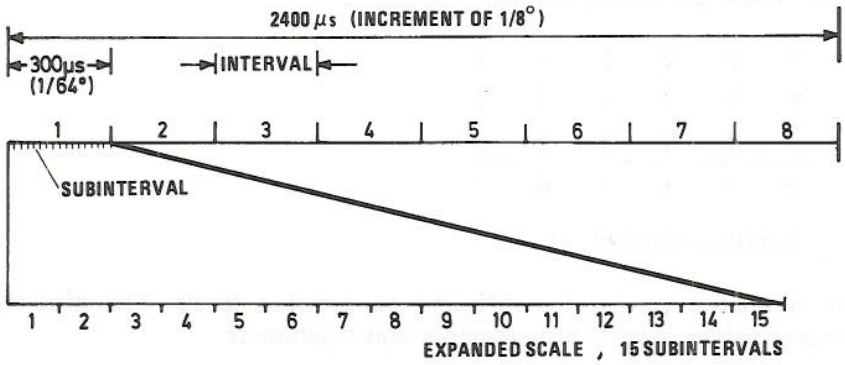

Figure 11.16 Division of an antenna incremental movement in azimuth of 1/8° into intervals and subintervals

4 The new weight distribution W_n is set at the end of the interval.

5 Steps 2, 3 and 4 are carried out for intervals 2 through 7. For interval 8 step 2 is repeated.

The new algorithm reduced the simulation time to about 1/10 of the previous procedure. The results showed that the difference in obtained suppression was only about 1/10 dB. Hence, for the rest of the simulations this simplified algorithm was used.

To make the simulation more realistic, two error sources were introduced:

- Error in the measurement of direction to the jammers. This error is assumed uniformly distributed with a maximum value $\pm\Delta\alpha$. $\Delta\alpha$ is an input variable to the program.
- Error in the measurements of noise power P_{out}. This error is also assumed uniformly distributed and limited to a maximum value $\pm\Delta P$. ΔP is an input variable to the program.

11.8 Number of bits for adaptive loop operation

In order to reach the minimum noise power level as quickly as possible, it is important to match the parabola to the actual curve as well as possible, such that the calculated K_{min} is close to the optimum value. The match is best for K_1 close to K_{min} and worst when the real minimum point is close to the extreme points 0 or K_2 or outside these points.

The values of K_1 and K_2 are functions of the number of bits M the adaptive loop is allowed to operate on. This number is expected to be greatest at the beginning of the iterations and to be decreasing as the minimum noise power level is approached. M is a function of number of iterations and noise power level and is an important parameter.

After some introductory simulations three distributions A, B and C were picked out for closer examination. These are tabled below:

A:	3	3	2	2	1	1	1
B:	4	3	3	2	2	2	2
C:	5	4	4	3	3	2	2
	1	2	3	4	5	6	7

Iteration number →

Figure 11.17 shows simulated results for different suppression levels. The plotted curves represent averaged values over 188 increments and 5 jammers.

Although there seems to be little difference in the results between sequence A, B or C, sequence C seems to give the best results for high initial noise power levels, indicating that the bit destribution preferably should be determined on a power level basis rather than iteration number.

This led to some simulations where the bit number M was determined according to the curves in Figure 11.18. The designations M=4, 5 and 6 refer to the number of bits at −60 dB level.

A typical attenuation characteristic is shown in Figure 11.19. The differences between the different curves are hardly significant but M=4 is preferred since the curves for both M=5 and M=6 show tendencies to oscillations.

11.9 Number of bit requirement for P_0 measurements

In the previous chapter it was assumed that the output noise power level was measured with infinite accuracy. However, P_o is also determined digitally with a finite word length, and quantization error will influence the operation of the adaptive loop.

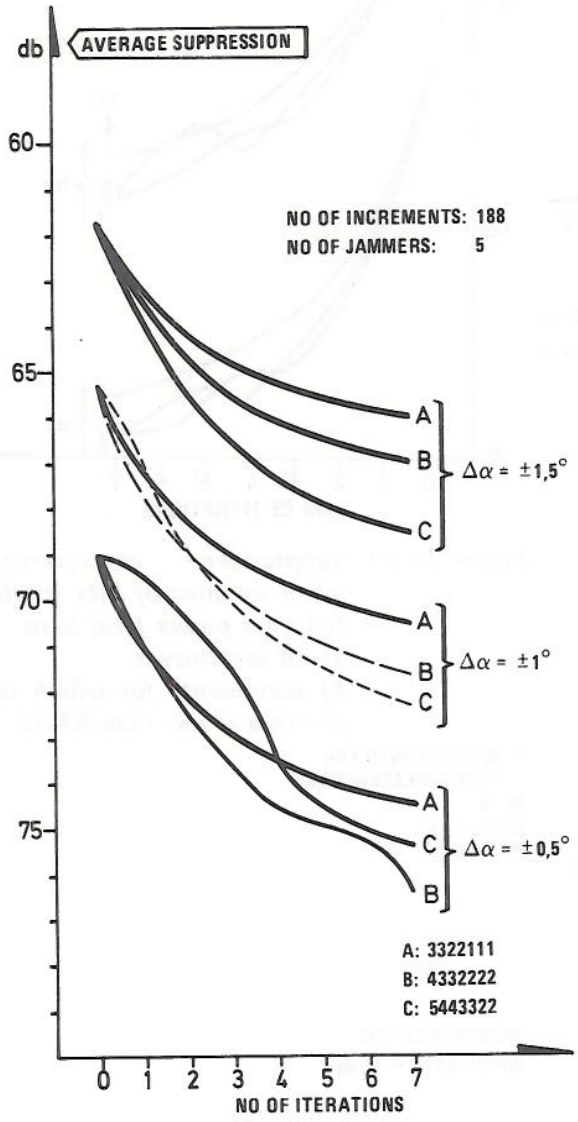

Figure 11.17 Average suppression as function of number of iterations

Based on an estimated maximum threat, the required suppression of the jamming noise power to reduce it to the thermal noise level is approximately 70 dB relative to the main lobe maximum gain. That is

$$\sum_{i=1}^{5} 10 \log (P_i) = -70 \text{ dB} \quad (11.1)$$

where P_i is the normalized power level (relative to the main lobe).

When the total noise from all five jammers approaches that level, the accuracy of the jamming power level measurement is greatly reduced. This means that the maximum average suppression of each jammer is approximately −77 dB, which may be below thermal noise level.

Figure 11.20 shows simulated results of average suppression for various word lengths for power output measurements. These results indicate, surprisingly, that the word length is a critical parameter and that 12 bits seem to be a requirement if full benefit is to be gained from the adaptive loop.

It is felt that additional simulations should be carried out to confirm these results.

As previously stated, the gradient was determined by changing the least significant bit in the weight setting. In the presence of noise it is expected that the gradient can be determined more accurately if larger steps are made. A new variable ℓ was introduced into the program defining the step size ΔW, given by

$$\Delta W = \ell \cdot \Delta W_{min} \quad (11.2)$$

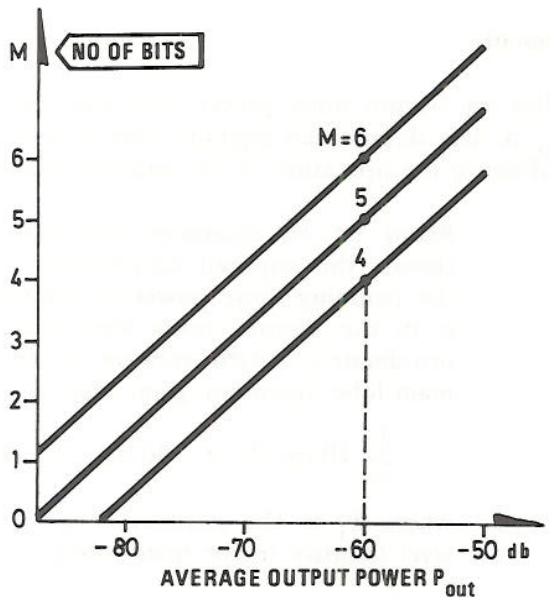

Figure 11.18 Selection of number of bits as function of output power level

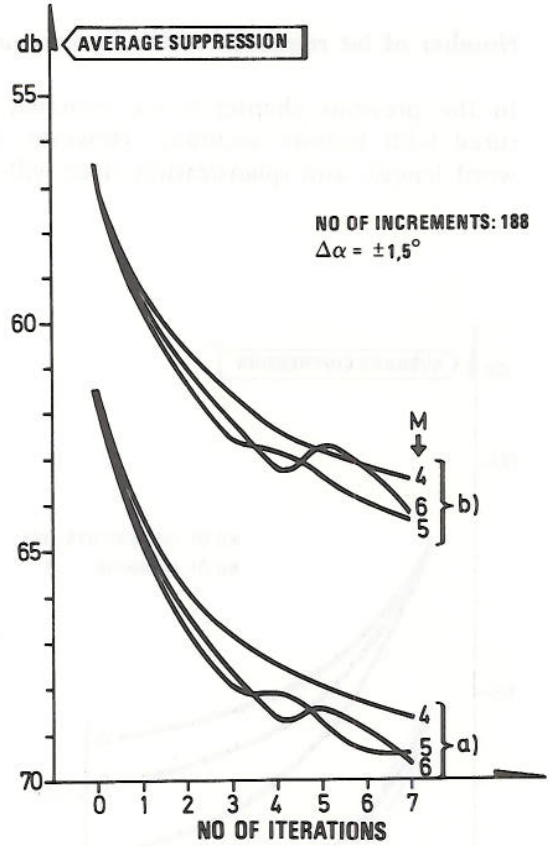

Figure 11.19 Suppression characteristics when number of bits is selected on a power level basis
a) all increments
b) increments for which suppression is less than 65 dB

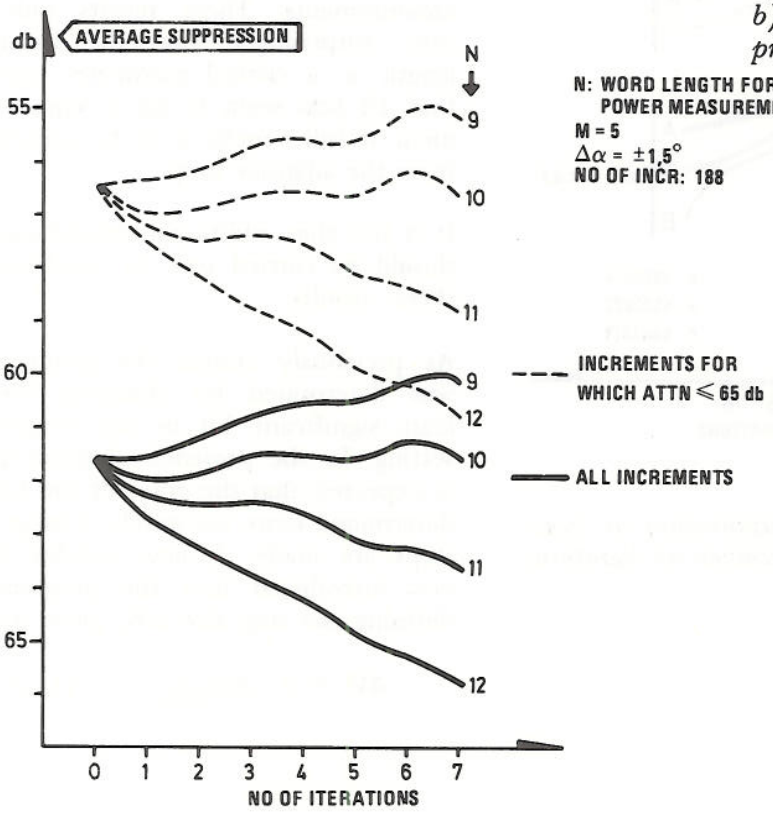

Figure 11.20 Suppression characteristics for different word length of power measurements

where

$$\Delta W_{min} = 2^{-N_F}$$

and

N_F = No of fractional bits

The simulated results presented in Figure 11.21 show that there is a marked improvement with increasing ℓ up to a factor of 4–5.

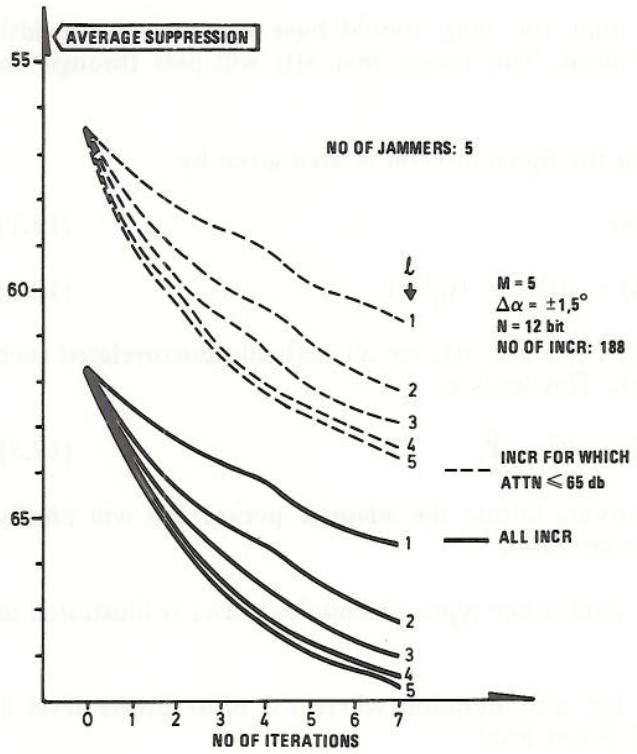

Figure 11.21 Suppression characteristics for different step size $\Delta W = \ell \cdot \Delta W_{min}$

12 ADAPTIVE LOOP OPERATION IN THE PRESENCE OF TARGET SIGNAL RETURNS

In section 3.2 it was assumed that the output signal y(t) contained jamming and thermal noise only. When a desired signal s(t) also is present, a firm requirement must be that the adaptive loop should not reduce the desired signal power appreciably.

The target signal form contained in $\overline{\epsilon^2(t)}$ depends on the correlator bandwidth. Large integration time constants will smooth the output signal and suppress all impulse type waveforms, also a target return.

A comprehensive study of the bandwidth requirements and other aspects of the adaptive loop performance is given in (16).

The developed algorithm suggests that the loop should have the same bandwidth characteristics as the radar receiver itself. This means that S(t) will pass through the correlator undistorted.

The total output power $\overline{\epsilon^2(t)}$ during the signal interval is then given by

$$\epsilon^2(t) = y^2(t) - N_R^2(t) \tag{12.1}$$

$$= [N_t(t) + N_j(t) + s(t)]^2 - N_R^2(t) \tag{12.2}$$

Again it can be assumed that $N_t(t)$, $N_j(t)$ and s(t) are all mutually uncorrelated such that all cross-correlation terms vanish. This leads to

$$\overline{\epsilon^2(t)} = \overline{N_j^2(t)} + \overline{s^2(t)} = P_j^2 - \overline{P_s} \tag{12.3}$$

The relative power ratio P_s/P_j is varying during the adaptive period and will ideally approach the undisturbed signal-to-noise ratio.

The influence of the desired signal (and other types of impulse noise) is illustrated in Figure 12.1.

The illustration is appropriate for the n'th iteration where the noise power level is reduced far below the desired signal power level.

The illustration applies to a CW transmitted pulse of 10 μs length. The reflected pulse from a point target will be of the same length and fill a time slot of 10 μs. In the illustrated case the signal pulse happens to appear in the middle of a time slot (No 4) where the power output is measured. Evidently this will introduce errors in the computed gradient for that particular iteration. Errors would also be introduced if the returned pulse appears in time slots 1, 12 or 13.

Large variation in output power for incremental changes in a single weight are, however, not likely. If the output power difference from one measurement to another exceeds a predetermined level, the last measurement is assumed to be either an impulse type noise or a target signal and may be disregarded. The exclusion of one power measurement is not expected to influence the calculated gradient appreciably. The situation is more difficult if a signal pulse appears in time slot 12 or 13 since here large output power errors may occur. A logical method to resolve this problem is to take two or three successive sampling points of P_{k1} and P_{k2} and observe the

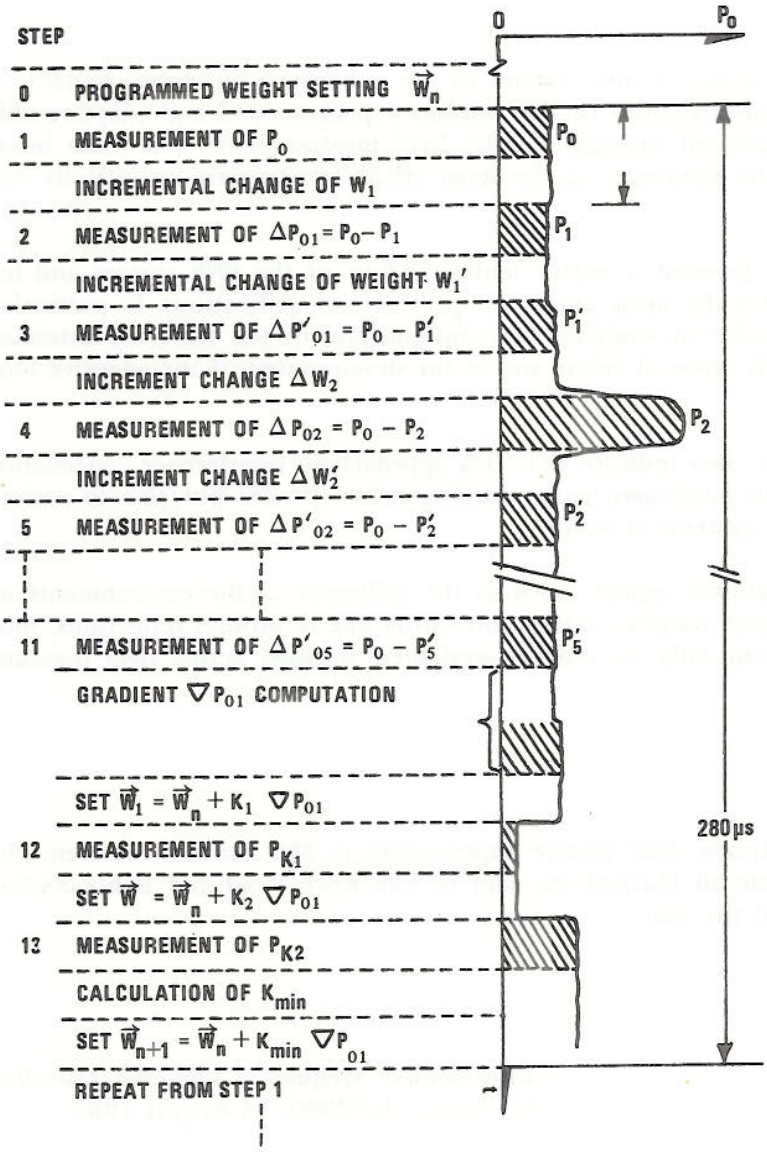

Figure 12.1 Example of one iteration when a target signal is present

measured power variations. Based on certain criteria a procedure can be developed which enables a logic circuit to sort out the actual noise level.

It is important to realize that as long as the adaptive loop algorithm is based only on true noise measurements its operation will not affect the desired signal power.

The procedure outlined above implies that the adaptive loop will not act on impulse type noise entering through the antenna side lobes. This type of interference cannot be handled by the adaptive loop but can be reduced through the normal programmed nulling and can also be effectively eliminated by the use of the well-known side lobe blanking technique.

13 CONCLUSION

The present feasibility study is not meant to be exhaustive in every respect. A number of operational uncertainties of the combined programmed and adaptive null-steering can only be disclosed through realistic field measurements. The main intention of the work was to elaborate on the most critical parameters analytically and through simulations.

The study has brought forward a better understanding of the PNS system and has established a platform for the most important parameter specifications. In particular, the work has been valuable in studying the configuration of the auxiliary antennas, the influence of different types of errors and in the development of the adaptive loop algorithm.

The results of this study also indicate that this approach to interference cancellation is applicable not only to land-based early warning radar systems but also to various types of communication systems as well.

More complicated operational aspects such as the influence of the environments on the main antenna radiation pattern, calibration errors due to ground reflections, multipath and clutter etc can only be reliably evaluated through actual field measurements.

Acknowledgements

The authors wish to express their sincere appreciation to Mrs Marit Støversten who kindly and skilfully made all illustrations, and to Mrs Ruth Sand and Bente Sæther who typed and processed the text.

References

(1) Howels, P A — Intermediate frequency side-lobe canceller, US Patent 3202990, 24 August 1965

(2) Applebaum, S — Adaptive arrays, SPL TR 66-1, Syracuse University Research Corporation (1966)

(3) Brennan, L E — Adaptive antenna processing and MTI technique, Course note, Technology Service Corporation, March (1973)

(4) Bryn, F — Optimum signal processing of three-dimensional arrays operating on gaussian signals and noise, *J Acoust Soc Amer* 34, 3, 289–97 (1962)

(5) Mermoz, H — Adaptive filtering and optimal utilization of an antenna, US Navy Busan of Ships (translation 903 of PhD thesis, Institute of Polytechnique, Grenoble, France (1965)

(6) Shor, W W S — Adaptive technique to discriminate against coherent noise in a narrow-band system, *J Acoust Soc Amer* 39, 1, 74–8 (1966)

(7) Widrow, B et al — Adaptive antenna system, *Proc IEEE* 55, 12 (1967)

(8) Griffiths, L J — A simple adaptive algorithm for real-time processing in antenna arrays, *Proc IEEE* 57, 10 (1969)

(9) Eggestad, M — Effektive elektroniske beskyttelsestiltak kontroll- og varslingssystemene, Teknisk notat E–777, Forsvarets forskningsinstitutt (1970) Confidential

(10) Eggestad, M — Forskjellige metoder til radarantenners sidelobeundertrykking og andre aktuelle emner i forbindelse med videreføring av "TOR", Reiserapport E–204, Forsvarets forskningsinstitutt (1977) Confidential

(11) Gabriel, W F — Adaptive arrays – An introduction, *Proc IEEE* 64, 2 (1976)

(12) Reed, I S
J D Mallet — Rapid convergence rate in adaptive arrays, *IEEE Trans AES* 10, 6 (1974)

(13) — Hughes Aircraft information

(14) — Compensated digital attenuator keeps phase shifts to ±3 degree over 80 dB range, *Microwaves* 8, 9, 107 (1978)

(15) Heier, S — Simuleringer i forbindelse med programmert nullstyring av en 3D radarantenne, Teknisk notat E–909, Forsvarets forskningsinstitutt (1977) Ugradert

(16) Anderson, R — Simuleringer i forbindelse med programmert nullstyring – Alternativ modus – av en 3D radarantenne, Teknisk notat E–1011, Forsvarets forskningsinstitutt (1978) Ugradert

(17) Forssell, B — Programmert nullstyring, Systemanalyse av adaptivdelen, STF44 F79137, Elektronikklaboratoriet NTH, Trondheim (1979)